Development of clickable approaches to build functional polymeric nanoparticles

Makawitage Daminda Ayal Perera, BSc.

The University of Nottingham

School of Pharmacy

Nottingham

UK

Thesis submitted to the University of Nottingham

for the degree of Master of Research

September 2009

To my

Parents and friends

Abstract

Smart functional nanoparticles have attracted considerable interest over the last few years due to their unique properties and behaviours, which could be used in a wide range of applications such as diagnostics and drug delivery.

Nanoparticles based on polyacrylamide matrices were constructed using free radical polymerisation methodology. Moreover, newly designed azido, alkyne and maleimido functional groups bearing nanoparticles were synthesised, and their unique chemical properties were comprehensively evaluated.

The contribution of monomer composition to the size distribution of particles was studied. The availability of the newly introduced functional groups was confirmed by clicking fluorogenic substrates followed by spectroscopic studies.

Acknowledgements

I would like to express my sincere gratitude to my supervisor Dr. Weng C. Chan for his valuable advice and support throughout this work and Dr. Jonathan Aylott for his help and guidance in the nanoparticle synthesis.

I would also like to thank Dr. Katharina Welser for her guidance on preparing azido and alkyne bearing nanoparticles.

Thanks also go to my lab colleagues Cillian Byrne, Sophia Salta, Gavin Hackett, Alex Trumen, Andy Mitchell, Robert Pineda and Leo Marques for their help and assistance.

I would especially like to thank Lee and Graeme, Paul and all the technicians who have given their time, their knowledge and resources in medicinal chemistry CBS laboratories and Boots building.

I would also like to thanks all my friends in CBS Adnan, Dan, Mike, Sara, Gopal, Ram, Charles, Ross, Geetha, Shailesh, Austin and the CBS cricket team members and everyone else for happy and relaxing moments while at the University of Nottingham. Thanks to Graeme Parry and Ally to accommodate me at their house.

Finally, special thanks to my father and mother in Sri Lanka for their endless support, encouragement, funding and without whom it would be impossible to complete this work.

Contents

List of Schemes

List of figures

List of tables

Abbreviations

APS	ammonium persulphate
Boc	*tert*-butoxycarbonyl
Brij 30	polyethylene glycol lauryl ether
Calcd.	calculated
conc.	concentrated
D_2O	deuterium oxide
DCM	dichloromethane
DCC	*N*, *N*-dicyclohexylcarbodiimide
DIAD	diisopropyl azodicarboxylate
dil.	dilute
DLS	dynamic light scattering
DMF	*N*, *N*-dimethylformamide
DMSO	dimethylsuphoxide
EtOAc	ethyl acetate
EtOH	ethanol
FTIR	fourier transform infra-red
^{1}H NMR	proton NMR
HPLC	high performance liquid chromatography
M^+	molecular ion (positively charged)
MeCN	acetonitrile

MeOH	methanol
MH^+	protonated molecular ion
mL	millilitre(s)
mmol	milli moles
mol	moles
m.p.	melting point
nm	nanometer
nM	nanomolar
NP(s)	nanoparticle(s)
NMR	nuclear magnetic resonance
PBS	phosphate buffered saline
TBTA	tris[(1-benzyl-1H-1,2,3-triazol-4-yl)methyl] amine
THF	tetrahydrofuran
TLC	thin layer chromatography
TAMRA	5-carboxytetramethylrhodamine

Chapter 1

Introduction

1.1 Optical nanosensors

Optical nanosensor technology has become widespread during the last two decades and has been applied to many fields of research including drug delivery[1], bioimaging[2] and biosensing.[3] The nanosensors (Figure 1.1) can be diverse in structure, and can be utilised for monitoring a variety of analytes.[3] For example these nanosensors can possess an inert biofriendly matrix containing highly sensitive fluorescent reporter molecules that relay analysis information in real-time. These nanosensors have dimensions less than 1 µm and can transduce chemical or biological events as optical signals.[4]

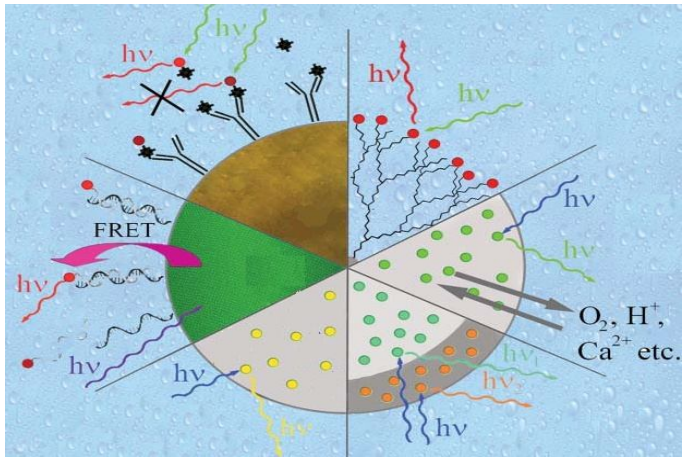

Figure 1.1: Schematic representation of nanosensors (reproduced from Borisov *et al*) [3]

Kopelman and co-workers introduced the concept of Probes Encapsulated By Biologically Localized Embedding (PEBBLE) in 1998 using the advantages of optical fibre based sensors.[5] Normally, the size of a nanosensor is less than 100 nm in diameter and can be inserted into cells with minimal physical

perturbations. If it is higher than 200 nm it can cause physical damage to the living cells.[4] Earlier technology relied upon the direct cell loading of fluorescent dyes. However, newly made optical nanosensors have several advantages over this method[4]. These advantages are:

(i) Ability to measure a high number of analytes are not limited to the use of a single fluorophore and have the ability to interact with enzymes, reporter dyes and ionophores to increase sensitivity, specificity and other beneficial aspects of the complete probe.

(ii) The intracellular environment is protected from any potential toxic effects that the sensing dye may cause by the nanoprobe matrix.

(iii) The sensing dye is protected from possible interference from cellular substances such as nonspecific binding proteins and organelles.

(iv) Able to carry out ratiometric measurements

Recently, three different types of matrices have been applied for the fabrication of optical nanosensors. These matrices are based on cross-linked poly (decyl methacrylamide) (PDMA), cross-linked polyacrylamide, and sol-gel silica.

Cross-linked poly(decyl methacrylamide) (PDMA) nanoparticles have been used for measure dissolved glucose level and have particle sizes in the 125-250 nm range.[6] Sol gel nanosensor matrix is known as silica sol-gel and has chemically inert optical transparent materials. Sol gel nanosensors PEBBLEs also designed to measure dissolved oxygen level in cells and also used to measure various ions such as zinc[7] and pH [8] and have 200-300 nm particle sizes.

The polyacrylamide based nanosensors are made of polyacrylamide matrix and have been used to measure analytes including zinc[7] and recently glucose level.[9, 10] These particles are typically less than 100 nm and have the advantage of minimal cell perturbation in cellular analysis over the above mentioned matrices. These newly designed nanoparticles have been applied in many fields and some of their uses are explained in following section.

1.2 Recent applications of optical nanosensors

Recently several kinds of nanosensors have been developed to detect various events of the cells and their functions.

1.2.1 pH sensor nanoparticles

The sensor nanoparticles are known to report relative fluorescence according to the pH value of the samples, to which they are exposed, within a specific pH range. pH related fluorescence is relatively simple to monitor.[11, 12] For example these nanosensors can be used as diagnostic devices to generate valuable information for stem cell biology. These stem cells have the capacity of extensive self renewal and as the origin of highly differentiated cells and tissues. Mesenchymal cells (MSC) are multipotent cells and found in adult marrow. Because of unique properties of nanosensors, it is easy to gather quantitative and robust data from hundreds of thousands cells and cell systems. Most interestingly it is possible to trace the movement of nanosensors of mother to daughter cell lineage using flow cytometry. This shows that during proliferation of nanosensor-loaded cells, daughter cells end up with equal numbers of nanosensors (per cell). From this evidence it is easy to measure the cell division time and can easily study cell behaviours and cytoplasmic split during mitosis.[13]

pH nanosensors can be used to monitor the effect of antimalarial drug chloroquine on the pH of the lysosome (which is involved in phagocytosis process). These pH nanoparticles are absorbed by murine macrophages by phagocytosis and then to the lysosomes.[11]

1.2.2 Glucose nanosensors

The glucose nanosensors are a kind of enzymatic PEBBLE biosensor using a co-immobilised oxidase enzyme .[9] Monitoring physiological levels of glucose in blood is important, since glucose has a primary relationship with diabetes mellitus and other diseases.[14] Electrochemical glucose microsensors could be used to measure the fluctuations of glucose in the extracellular space of single islets of Langerhans and the glucose consumption by pancreatic beta cells.[15] But the newly designed glucose sensitive PEBBLEs are further advancing this

measurement technology by enabling *in vivo* measurement of intracellular glucose. [9]

1.2.2.1 Mechanism of glucose sensitive nanosensor

So far various types of optical nanosensors have been made using polyacrylamide matrixes. The most recent ones are glucose nanosensors. These PEBBLEs are highly sensitive to glucose in the sample, which is oxidized to gluconic acid. This is done by the glucose oxidase enzyme in the PEBBLE particles. Oxygen is consumed directly in this process and at a selected time oxygen level is lower than the reaction start time. This oxygen concentration level difference results in the ruthenium dye $(Ru\{dpp(SO_3Na)_2\}_3)Cl_2$ undergoing less quenching. Therefore emitted luminescence is increased. The ruthenium dye expresses the change in oxygen concentration *via* a change in luminescence.[9]

These PEBBLEs contain special dyes (Texas red-dextran/ Oregon green 488-dextran) included in the polyacrylamide matrix, giving a ratiometric measurement of the glucose concentration *via* a change in fluorescence. The main purpose of these dyes is to make the PEBBLEs ratiometric in both the emission and excitation modes. Texas Red-dextran is used in conjunction with $(Ru\{dpp(SO_3Na)_2\}_3)Cl_2$ to get the fluorescence spectra for excitation-based ratiometric measurements, using a ratiometric excitation method based on utilizing Texas Red as the reference dye. The emission from both dyes overlaps and the excitation band from each dye can be spectrally resolved. Therefore the excitation filters can change at a rapid rate and the emission collected[9]

However, without a proper method to deliver nanosensors to the targeted cellular region, all the benefits of nanosensor technology will not be realised. Delivery methods of nanosensors are discussed briefly in the following section.

1.3 Delivery methods of nanosensors to the intracellular environment.

Nanosensors are mainly designed for use in intracellular analysis. There are various introduction methods used for the specific cell system and it is important to retain cellular viability. These techniques include picoinjection[16], gene gun delivery[17] and the use of cell-penetrating peptides (CPP).[18]

1.3.1 The gene gun system

The gene gun system was first described by Sanford *et al*. This instrument is primarily used for the transfection of cell cultures with DNA or bacterial plasmids for genomic manipulation. The gene gun has also been used as a delivery method to transfer synthesized nanosensors into the cells. Using gene gun, nanosensors are propelled into the cell culture dish, embedding them randomly into adherent cells. However, there is no control of positioning of the sensors. When applying the gene gun method, correct pressure and particle concentrations must be maintained for effective results. Gene gun bombardment has been used to insert oxygen nanosensors containing the oxygen-sensitive fluorophore $Ru\{dpp(SO_3Na)_2\}$ along with the reference dye Oregon Green into cells.[16, 17]

1.3.2 Picoinjection

Picoinjection has been used to inject picolitres of fluids in to a single cell. This technique is mainly used for *in vitro* fertilization and for directing drug injections to specific cell areas. The picoinjection method is used to inject a suspension of PEBBLE to study the several stages prior to the hatching of embryos. The drawbacks of this method include the necessity of highly skilled individuals to insert the sensors into the cells without undesired perturbation.[16]

1.3.3 Cell penetrating peptides (CPP)

The plasma membrane of eukaryotic cells acts as a great protector for the cell from potentially hazardous foreign bioactive molecules. Protein-based drugs and other small molecules are not endogenous to the cell. Therefore the plasma membrane refuses most kinds of exogenous molecules entry into the cell. This is important to keep in mind when applying pharmaceutically active agents and drugs to cell cultures or during *in vivo* testing. In the late 1980s and early 1990s, there was a major breakthrough in the discovery of transporters, that can efficiently cross the plasma membrane.[19] This significant identification was the Tat peptide. This peptide is derived from the HIV Tat trans activator protein. The full-length of this tat peptide can cross the plasma membrane and small fragments of this peptide can also easily enter into cells. These kinds of

molecular transporter peptides are known as cell-penetrating peptides (CPPs).[18, 20] Nowadays biochemists and chemists alike have designed many variations of internalising peptide structures. They have also used biophysical methods to characterize the mechanisms underlying cellular uptake. Tat or other Tat related CPPs have been developed by researchers to transport a variety of intracellular cargoes into cells including DNA,—polymers, nanoparticles and liposomes[21]. So these Tat related CPPs are used as a powerful tool for transporting diverse materials across the cell membrane.[22]

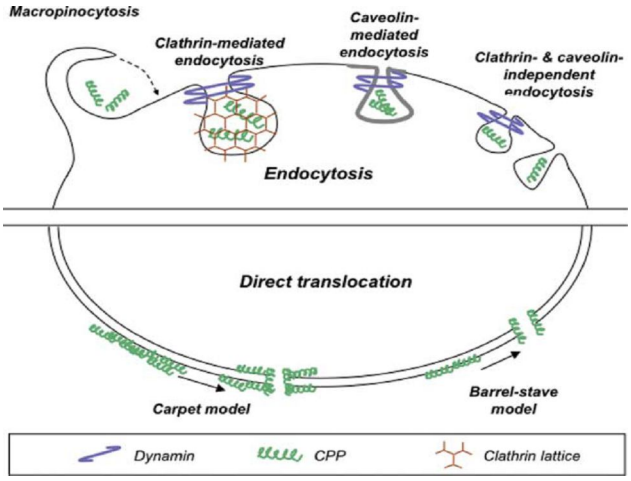

Figure 1.2: Mechanisms of uptake of Tat peptide across the plasma membrane. (Reproduced from Stewart *et al*). [18]

CPP uptake by cells is highly dependent on the properties of the CPP used and the attached cargo particles such as the chemical properties, peptide length, and size. CPPs can enter into a cell by two different routes (Figure 2). Utilising either endocytosis (energy-dependent vesicular mechanisms) involving the translocation of the lipid bilayer.[18] Fluorescence imaging is useful for visualizing tissues *in vivo* and relies on tracking molecular imaging agents. CPP conjugates with various fluorophores have improved stability and have been developed as imaging agents. For example, fluorescein doped monodispersed silica particles (which have an approximate diameter of 70 nm) modified with Tat peptides for cellular delivery have the ability to cross the blood brain barrier efficiently.[23] Most importantly, CPP modified agents do not appear to interfere with biological function as other particles can do.

Nanoparticles which bind to Tat in stem cells do not trigger an immune response.[18]

1.4 Synthesis of nanoparticles

All polyacrylamide PEBBLEs, which are the focus of this thesis, are synthesized in inverse-microemulsion systems. These microemulsions classified as water in oil (w/o) according to the dispersed and continuous phases. Normally the size range of 10–100 nm monodispersed droplets are containing in dispersed phase.[24-27]

1.4.1 Inverse microemulsion system

Great attention has been given to polymerisation in microemulsion during last two decades. There are several advantages of microemulsion over the macro and miniemulsion. Both these macro and mini emulsions are thermodynamically unstable and opaque while transparent and thermodynamically stable systems can be seen in microemulsion. Most importantly the dispersion size of the microemulsion is below 100 nm and mainly consists of three major components. Two components are immiscible liquids and the third one is always a surfactant. These surfactants are used to stabilize the microemulsion and to control the particle size. Microemulsion is mainly based on the composition of the oil and water percentage of the system.[28] For example, oil in water (o/w) has high amount of water, while water in oil (w/o) has less water.

Inverse microemulsions are considered as water in oil (w/o) system and are ideal to carry out polymerisations to make thermodynamically stable nanoparticles in the range of 20-50 nm. These nanomatrices are particularly suitable for applications such as drug delivery and biomedical diagnosis.

In the preparation of inverse microemulsion, surfactants are also added to the polymerisation mixture and there is a continuous oil phase and an aqueous dispersed phase thermodynamically compartmentalized by surfactants. These are in nanometre sized liquid entities and they are also known as micellar solutions.[29, 30] The surfactant molecule consists of two parts: a polar hydrophilic head group and a nonpolar hydrophobic tail (hydrocarbon chain).

In a W/O system, the hydrophilic groups are sequestered in the micelle core and the hydrophobic groups extend away from the centre. Surfactants give a specific microenvironment to acrylamide monomers for the polymerisation and also inhibit the polymerisation of different droplets during the reaction by acting as steric barriers. In these practices, the reverse micelles incorporate the cross-linking agent, fluorescent dyes, enzyme and the acrylamide monomers. The above mentioned are hydrophilic and they stay in aqueous layer of the micellar droplets. [29]

1.4.2 Polymerisation of acrylamide monomers in inverse microemulsion

Polyacrylamide gels can be produced by the co-polymerisation of acrylamide and bis-acrylamide monomers.[31] This polymerisation is a vinyl addition polymerisation.[32] It is initiated by a free radical generating system which consists of ammonium persulfate (APS) and *N,N,N',N'*-tetramethylethylenediamine (TEMED). The original free radical is produced by the homolysis of APS, and TEMED is used to accelerate the formation of free radicals. Therefore, TEMED in turn catalyses the polymerisation. These activated ammonium persulfate free radicals start to convert acrylamide monomers into activated acrylamide monomer free radicals. [31] This process is known as the polymerisation initiation step. Then activated acrylamide monomer free radicals start to react with acrylamide monomers to begin the chain propagation step. These elongating polymer chains are randomly bound with bisacrylamide monomers to crosslink other acrylamide polymer chains. This results in the characteristic porosity of the polyacrylamide matrix. [33]

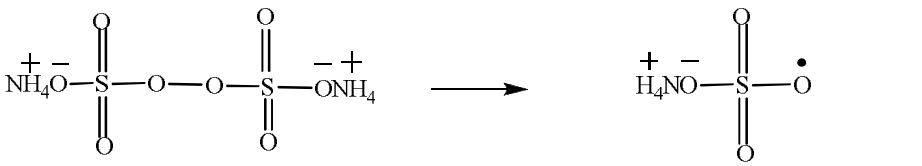

ammonium persulfate ammonium persulfate free radical

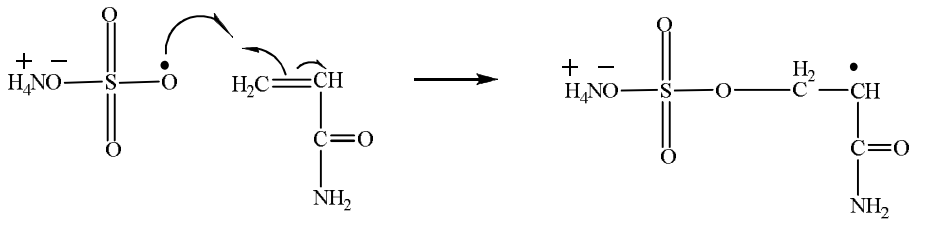

unactivated acrylamide monomers activated acrylamide monomer free radicals

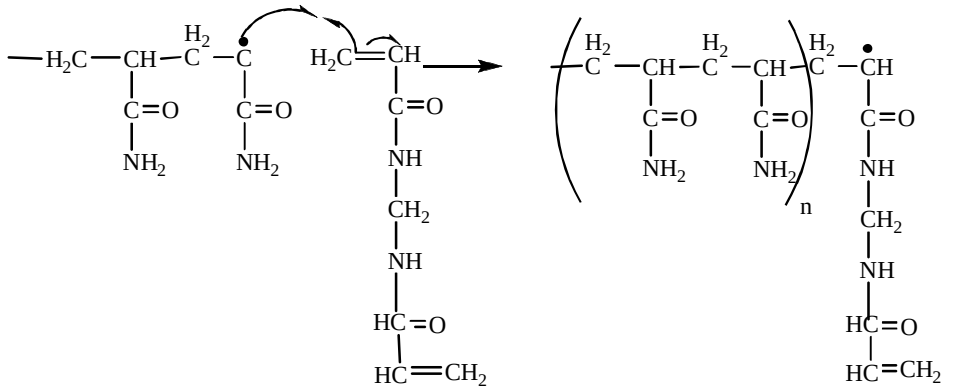

bis-acrylamide monomer activated bis-acrylamide monomer

Schemes 1.1: Polymerisation of acrylamide monomers in microemulsion.

Concentration of the initiators has an effect on polymerisation, the rate of polymerisation depends on the concentration of the initiators. However, when the concentration of initiators is high (e.g. ammonium persulfate and TEMED) the rate of the polymerisation is increased. This therefore results in the decrease in the average polymer chain length and an increase in gel turbidity. Sometimes, excess initiator can produce a gel solution that does not appear to polymerise.

Oxygen can act as an inhibitor for the acrylamide polymerisation. The formation of polyacrylamide gels proceeds *via* free radical polymerisation and the presence of oxygen can inhibit any element or compound that serves as a free radical for the reaction. Hence, these reactions must be done in a oxygen free atmosphere (i.e. under argon).[34]

The polymerisation of acrylamide occurs in the aqueous cores of the micelle in the inverse-microemulsion, the sizes of which are dependent upon the concentration of surfactants. Varying this concentration will result in an

alteration in nanoparticle diameter. Experiments have also shown that the size of the nanoparticles can also vary with the solvent used, the monomer or the temperature of the reaction. Typically, the major surfactants are Brij 30 and dioctyl sulfosuccinate (AOT). If the surfactant concentration is high the nanosensor diameter becomes relatively smaller in size. Different types of techniques have been used for the characterization of these polyacrylamide nanoparticles. The sizes of the nanoparticles are normally characterized by the using dynamic light scattering (DLS) analysis.

DLS analysis can be used to determine the sizes of small particles in suspension or polymers in solutions. Particles and molecules in solution undergo Brownian motion. If these particles are illuminated with a laser, the intensity of scattered light fluctuates at a rate which depends upon the particle sizes. DLS measurements are highly accurate and reliable to analyse the particle sizes of polyacrylamide nanoparticles.

1.5 Proteases

Proteases are enzymes, and at least 500-600 proteases have been identified using bioinformatic analysis of the mouse and human genomes. These proteases have adapted to a wide range of conditions during their evolution. Food digestion and intracellular protein turn-over are considered as the primary roles of proteases. [35]

These proteases have the ability to hydrolyse peptide bonds. Their mechanisms for substrate hydrolysis are used to categorise them as serine, cysteine, threonine, aspartic, metallo or glutamic proteases. These proteases cleave protein substrates either from N-terminus (amino peptidase) or C-terminus (carboxypeptidase) or in the middle of the molecule (endopeptidase).[35]

Serine and threonine proteases hydrolyse protein peptide bonds by using their hydroxyl groups. The glutamic acid protease mechanism was not described until 1995 and very recently has been classified as the sixth catalytic type of peptide. The glutamic catalytic mechanism involves a water molecule which is activated as hydroxide ion by the carboxylate of a glutamate residue. This activated hydroxyl ion attacks the carbonyl carbon of the peptide bond and

results in the formation the tetrahedral intermediate. The side chain of amino amide of glutamate-53 stabilises the tetrahedral intermediate by forming oxianion and the protonation of the leaving group nitrogen is determined by the proton transfer from the glutamate-136 protonated carboxylic group. (Scheme 2).[36]

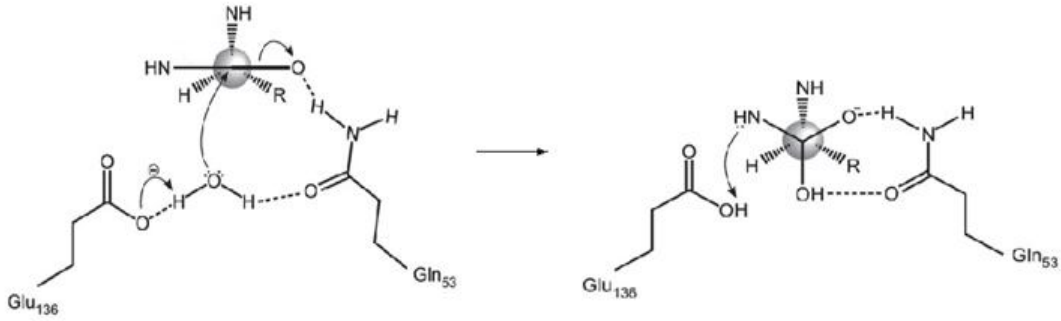

Scheme 1.2: Catalytic mechanism for glutamic proteases.[36]

Protease signalling pathways are very tightly controlled. When the regulation of a protease signal fails, it can lead to disease conditions. For example, serine proteases are key in thrombosis.[39] A great deal of research has been performed in order to directly visualise protease activity in cells.

1.5.1 Detection of enzyme activity

The study of the function and the behaviour of proteins both in a real environment and in real time is one of the biggest challenges. Screening their activities in real time makes it relatively easy to understand their activities and regulations within cells or tissue.

Recently, methods for the detection of enzyme activity have been developed and different types of fluorogenic substrates have been used to screen enzyme activities within cells. Most of these fluorescent substrates release photons over the enzyme-catalysed processes.[35] Once proteolytic cleavage occurs in peptidic scaffolds, a reporter molecule changes its fluorescence. This technology is being used to visualise common activities of the tissues. The main target of the fluorescence based analysis is to target specific proteases, e.g. Caspase-3 is the targeted protease for apoptosis.

1.6 Phenomenon of fluorescence

Molecules have various states of energy levels. Most molecules at room temperature stay in the lowest electronic level called the ground state (S_0), which is also the lowest energy level. These ground state levels can be excited to higher energy levels through the absorption of a photon. Once excited, they can be jumped up to S_1 or S_2. These excited molecules are unstable and will relax once more to a lower energy level by several de-excitation processes. The overall process is illustrated in the Jablonski diagram (Figure 3).[37]

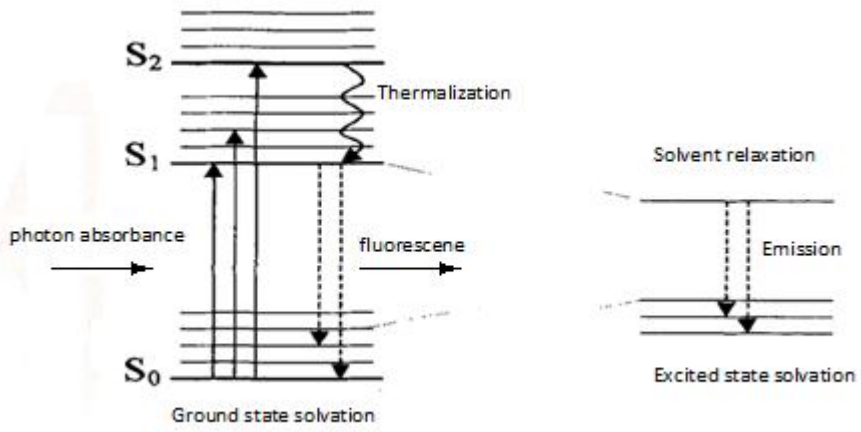

Figure 1.3: Jablonski diagram (modified from Croney *et al*). [37]

Normally the relaxation process occurs by transformation of the absorbed energy into heat or by emission of a photon. These excited molecules have the ability to collide with other surrounding solvent molecules and excess of vibrational energy can be transferred to the solvent. The ultimate result is the transition from S_1 to S_0 via internal conversion. Internal energy absorption is equal to the combination of vibrational and internal conversions. When relaxation from $S_1 \rightarrow S_0$ occurs through emitted photons, it is called fluorescence. For a given molecule, the fluorescence spectrum maxima have higher wavelengths (lower energy) than those relative to the absorption spectrum. This difference (Strokes shift) is due to the energy loss in the excited state caused by vibrational relaxation. Absorption of a photon is approximately as fast as the emission of a photon and 10^{-8} s is the typical lifetime of fluorescence. [37]

Fluorescence detection based analytical techniques have higher sensitivity and selectivity which make them a common technique for visualization of protease activities attached to fluorogenic substrates. These fluorogenic substrates can be designed in various ways.

1.6.1 Types of fluorophore substrates

Different types of fluorophore substrates have been designed over the last few years, such as the (i) internally activate substrates, (ii) fluorescence resonance energy transfer (FRET) and (iii) polymer based near infrared probes (NIRF probes).

(i) Internal activate substrates consists of a typical protease activity targeted peptide based reporter. Once the protease cleavage occurs, these peptide bound fluorophores emit fluorescent signals. For example, a tetra peptide (Asp-Glu-Val-Asp) which has the caspase-3 target peptide sequence has been designed and attached to a fluorescent 7-amino-4-trifluoromethyl coumarin, and can be used to detect the caspase activity in apoptotic cells.[38]

(ii) Fluorescence resonance energy transfer (FRET)-based probes have two fluorophores (acceptor and donor) placed closer than 100 Å to each other, where the excitation wavelength of the donor is overlapping the emission wavelength of the acceptor. Once protease cleaves the linker, the fluorophores are separated and this suppresses the transfer of energy between the two. This results in the increase of emission intensity of the donor while decreasing the emission of acceptor. These changes in fluorescence can be detected and monitored to determine the specific activity of the target protease.[38]

(iii) Polymer based near infrared probes have a near infrared fluorescence and contain a cleavable peptide spacer, fluorophore and a high molecular weight polymer, often a polyethylene glycol (PEG) graft co-polymer. These PEG chains have been known to disrupt the interactions between the target enzyme and the peptide substrate. Therefore, NIR fluorophores may not be efficiently cleaved.

Fluorogenic reporters are widely used for *in vivo* imaging.[38] Delivery of these polymer based near infrared probes is facilitated by the novel, long, synthetic

graft copolymers and have ability to accumulate in tissues and tumors. These graft copolymers contain lysine side-chains and are modified with cyanine-based dye Cy5.5. These modifications are done through protease sensitive peptide linkers. Cleavage of the amide bonds by proteases result in the increase in fluorescence intensity of the near infrared probes.[38] However, most of the time, these reporters suffer from drawbacks related to autofluorescence and the light scattering nature of the tissues. Polymer based near infrared probes can be used to overcome these limitations and are prefered for *in vivo* molecular imaging of living cells because of their longer wavelengths. Their longer excitation and emmiting wavelengths have a good tissue penetration and cause less photo-damage to cells. Longer wavelengths also produce less autofluorescence background, offer good sensivity and less light scattering than visible light.[38] Therefore, it is recommended for living cell imaging. These imaging reagents have allowed the non-invasive visualization of enzyme activity in whole organisms, e.g. TAMRA

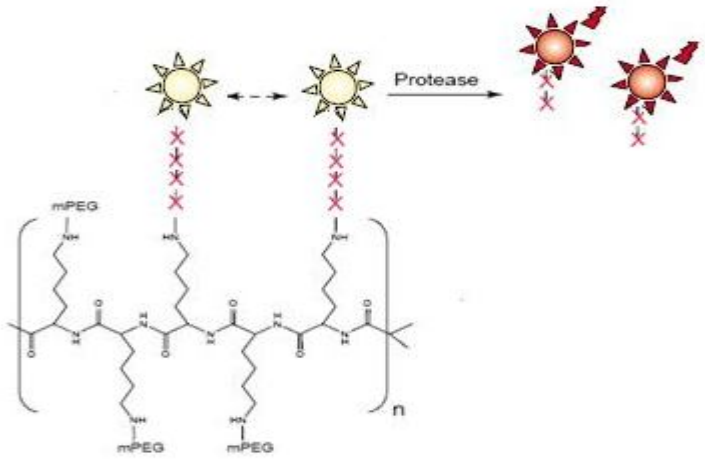

Figure 1.4: NIR fluorogenic reporters for *in vivo* imaging (modified from Baruch *et al*).[38]

The coupling methods of peptides and fluorophores are discussed details in following section 1.7.

1.7 Coupling of peptides and fluorophores with nanoparticles.

1.7.1 Coupling methods

During recent years coupling reaction methods have progressed significantly. In a typical peptide coupling reaction, the carboxylic acid moiety of a specific amino acid is first activated by a carboxylic activative reagent and then reacted with the amine group of the targeted amino acid. Development of new coupling reagents has accelerated past few years. Early years dicyclohexylcarbodiimide (DCC) had been used to activate the hydroxyl group of carboxylic acids. However, there are drawbacks on this method such as insolubility of urea co-product in most organic or aqueous solvents.[39]

To overcome these problems, new advanced peptide coupling reagents have been produced and high yields are expected from these newly designed coupling agents. Example of these reagents are O-(benzotriazol-1-yl)-*N*,*N*,*N'*,*N'*-tetramethyluronium tetrafluoroborate (TBTU) and 2-(1H-7-azabenzotriazol-1-yl)--1,1,3,3-tetramethyl uronium hexafluorophosphate (HATU)

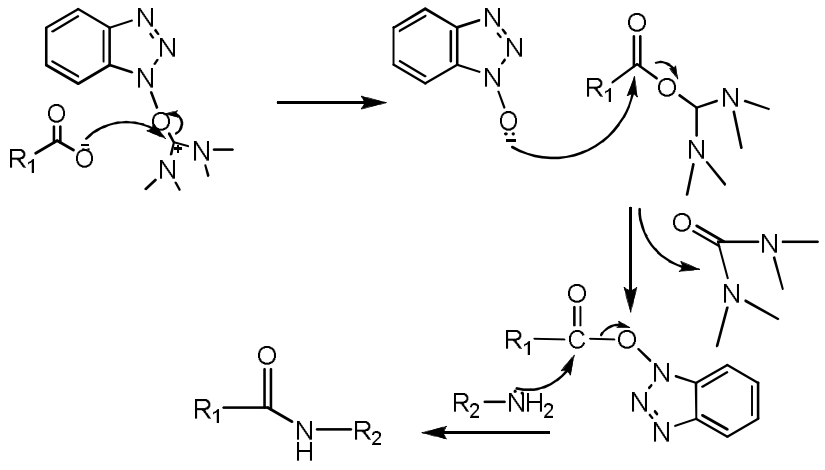

Scheme 1.3: The mechanism of carboxylic acid activation by TBTU.

The click reaction method which was frequently applied in the course of this work was a thiol-alkene click reaction, which is explained in more detail in following section.

1.7.2 Thiol-alkene click reaction

The Michael addition of a nucleophile to electron deficient alkenes is key a reaction in organic chemistry. The reaction between thiols and alkenes to form a carbon sulfur bond play an important role in biosynthesis. The sulfur atom of the thiol group is nucleophilic and fairly acidic. These reactions can be used for the identification of unknown alkene groups such as concentrations of unknown maleimides in a sample.

Maleimide is known for its high reactivity towards thiol groups. Cysteine contains a thiol group and its SH group reacts better with maleimide vinyl groups than with nucleophilic amino acids. For example, this reaction is faster than the addition of an amine to maleimide at pH 7 and below.[40] The high efficiency of this reaction makes it an excellent tool in the field of bioconjugation. These reactions can be catalysed by using tertiary amines such as diisopropylethylamine and triethylamine.

1.7.3 Huisgen Cu(I)-catalyzed azide-alkyne coupling (CuAAC)

Nowadays there are several bioconjugation reactions available. Recently, two chemoselective coupling reactions have been introduced: Staudinger reaction between azide and phospines and azide-alkyne couplings. In both of these cases azide moieties have been used. This group has unique features of its own. The azide functional group is very rare in natural compounds and has a high reactivity.[41-43]

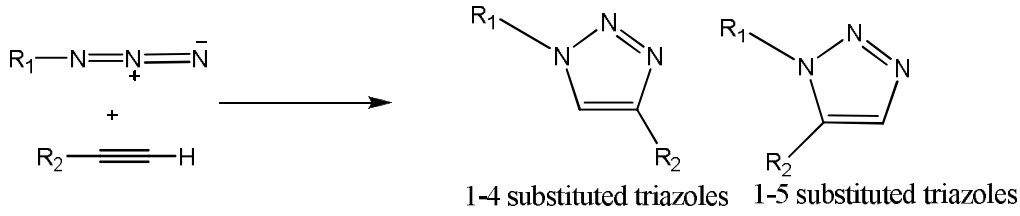

Scheme 1.4: Azide and terminal alkyne cycloaddition to give 1,2,3-triazole mixture with 1,4 and 1,5 substituted triazoles.[41]

Alkyne-azide reactions are also known as Huisgen cycloadditions. These result in the formation of 1,2,3-triazoles and are thermodynamically favourable reactions. However, uncatalysed azide alkyne cycloaddition have poor regiospecificity leading to a mixture of 1,4 and 1,5 substituted triazoles.[41]

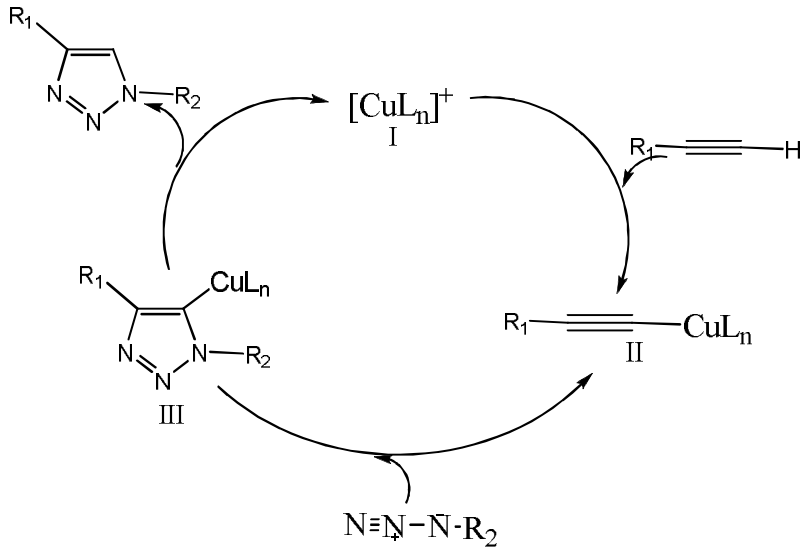

Scheme 1.5: Simplified proposed catalytic cycle for the CuAAC reaction.[42]

Copper(I) has important roles in chemistry and biology. It is widely used in a variety of organic coupling reactions. Copper(I) catalysts can be used in the Huisgen 1,3 dipolar cycloaddition to increase the speed of the reaction and also to ensure the regiospecificity. It promotes the reaction exclusively towards the 1,4-regioisomer of 1,2,3-triazoles with high yields.

CuAAC has a complex mechanism and its catalytic cycle has three major steps. The formation of Cu(I) acetylides is the first step of the catalysis of the CuAAC. In this step Cu(I) species activate the terminal alkyne to form a Cu(I)acetylide **(**II).[42, 43] Then the Cu(I)acetylide reacts with azide and form a Cu(I) triazole intermediate which is though to be formed through a six membered metalla-cycle.[45] The proteolysis of the Cu(I) triazole intermediate then results in the formation of the desired 1,2,3-triazole product and in the regeneration of the catalyst.[42] The Cu(I) catalyst drives the reaction exclusively towards 1,4-regioisomer of 1,2,3-triazoles.

Ligands like tris((1-benzyl-1H-1,2,3-triazol-4-yl)methyl) amine (TBTA) are often added to improve the CuAAC reactions. This might slow down the oxidation of Cu(I) to Cu(II) in the presence of traces of air while enhancing the catalytic activity.[43]

1.8 Aims and Objectives

Nanoparticles with polyacrylamide matrices could be readily obtained by free radical polymerisation.[24] Polymeric nanoparticles often display amine suitable for further NP chemical modification.[44] Due to their undesired tendency to aggregate, it is anticipated that the free amino groups in the nanoparticles can be replaced with designed functional groups to afford azido, alkyne and maleimido bearing nanoparticles.

In this thesis, optimisation of synthesis, the optimum composition of monomer feed related to the narrow size distribution and availability of the functional group will be studied.

Furthermore, the azido and alkyne bearing nanoparticles could be further modified by Huisgen Cu(I) catalysed azido-alkyne cycloaddition (CuAAC)[45] and the maleimide and vinyl ester functional groups bearing nanoparticles could be modified by thiol-maleimide[46, 47] click reaction.

The following chapter deals with:

- Development of azido bearing nanoparticles
- Development of alkyne bearing nanoparticles
- Development of maleimide bearing nanoparticles

Chapter 2

Results and discussion

2.1 Development of azido bearing nanoparticles

2.1.1 Introduction

Recent reports indicated that free amine-functionalised polymeric nanoparticles could be synthesised using amine-bearing monomers such as N-(3-aminopropyl)methacrylamide.[44] Due to the reactivity of the free amine group, nanoparticles were observed to aggregate over a period of time. The reactive free amino groups of N-(3-aminopropyl)methacrylamide nucleophilically attack the unreacted *N,N'*-methylenebisacrylamide and as a result undergo a Michael addition reaction with adjacent particles.[48] To overcome self aggregation of nanoparticles, these amine functional groups were replaced with azido functionalised monomers.

The azido functionalised monomer employed in this study is derived from poly(ethylene glycol) (PEG) and the properties of PEG can be exploited to improve the properties of nanoparticles, such as water solubility and increase the stability of bio molecules against degradation.[49]

These azide bearing nanoparticles have free azide functional groups on their structure and could be modified by the Huisgen Cu(I) catalysed azide-alkyne cycloaddition (CuAAC) reaction.[50] This click reaction can be performed in aqueous medium at room temperature. Hence, these nanoparticles can be used to click to other functional chemical groups which contain alkyne moiety at the terminal end *via* a CuAAC click reaction.[42]

2.1.2 Types of monomers

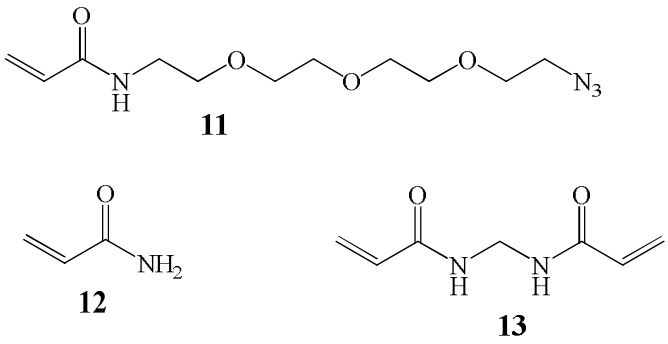

Figure 2.1.1: Monomers used to synthesise azido bearing nanoparticles

Hence, three types of monomers were used to synthesise the desired nanoparticles. They are acrylamide **12**, *N,N'*-methylenebisacrylamide **13** and *N*-(11-azido-3,6,9 trioxoundecanyl) acrylamide **11**. All the monomers have a single alkene functional group, and *N,N'*-methylenebisacrylamide has two alkenes, which can contribute to the cross-linking of the polymer matrix. The amount of *N,N'*- methylenebisacrylamide can effectively change the porosity of the matrix of the nanoparticles.[27]

2.1.2.1 Sources of monomers.

11-azido-3,6,9-trioxaundecan-1-amine **14,** acrylamide **12** and *N,N'*-methylenebisacrylamide **13** are commercially available and only *N*-(11-azido-3,6,9-trioxaundecanyl)acrylamide **11** was synthesised.

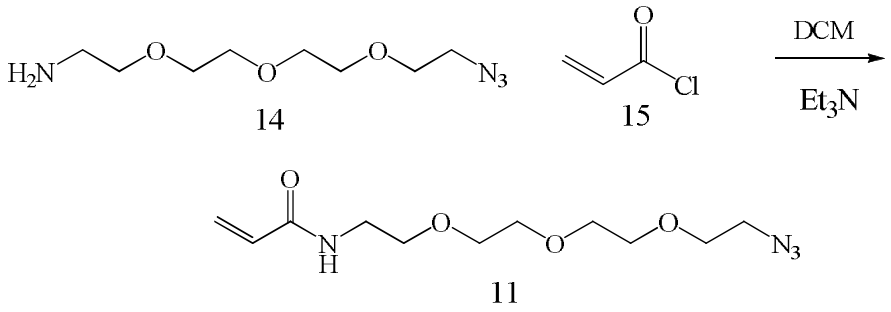

Figure 2.1.2: Acrylation of the amine azide derivatives

The building block, *N*-(11-azido-3,6,9-trioxaundecanyl)acrylamide **11** was obtained as a yellow coloured oil by the reaction of 11-azido-3,6,9-trioxoundecan-1-amine **14** (see section 4.2.1) and acryloyl chloride **15** (Figure

2.1.2). The co-product of this reaction was HCl, which can cause a decrease in the pH of the solution. Triethylamine was added as the base to neutralise the H^+ ion. The solvent DCM was then removed on the rotary evaporator and triethylammonium chloride was precipitated by adding THF and was filtered. THF was evaporated and a yellow coloured oil was obtained as the crude product. The product was separated by using RP-HPLC.

The success of the acrylation reaction was confirmed by ^{1}H NMR analysis. The peaks of acrylate groups (C=CH_{cis}, C=CH_{trans}, C*H*=CH_2) appear together with 11-azido-3,6,9-trioxoundecan-1-amine moiety confirmed the successful incorporation. The product was also analysed by ^{13}C-NMR and mass spectrometry.

2.1.3 Composition of monomers

The composition of the monomer feed can have a direct affect on the particle size of the nanoparticles. Adjustment of this parameter can result in particle sizes of between 10 nm and 100 nm.[25] During the synthesis process, different compositions of monomer feeds (Table 2.1.1) were used to investigate the optimum monomer feed with respect to the DLS analysis.

Table 2.1.1: The monomer compositions of azido bearing nanoparticles, synthesised by using different ratio of reactants and reacted for 2 hours.

Attempt	Amount of monomers (mg)				Recovered yield (mg)
	Maleimide	Acrylamide	Bisacrylamide	Expected yield	
1	20.0 (5.5%)	265 (72.6 %)	80 (21.9 %)	365	147
2	13.6 (3.8%)	265 (73.8 %)	80 (22.4 %)	358.6	229
3	13.6 (3.8%)	265 (73.8 %)	80 (22.4 %)	358.6	247.4
4	13.6 (3.8%)	265 (73.8 %)	80 (22.4 %)	358.6	258.4
5	12.5 (3.6%)	265 (73.8 %)	80 (22.3 %)	357.5	265

The amount of acrylamide **12** and *N,N'*-methylenebisacrylamide **13** were kept constant and the amount of azido functionalised monomer **11** was changed. According to the **Table 2.1.1**, yields were increased, when the azido functional monomer amount was decreased. The least amount of functionalised monomer resulted in the highest yield of the acrylamide polymerisation and polymerisation is described in the following section.

2.1.4 Polymerisation of nanoparticles

Inverse microemulsion system was used to synthesise the azido bearing nanoparticles. Here, the continuous phase was oil, which was hexane. The dispersed phase was water. The surfactant mixture was Brij 30 and AOT. Water-in-oil with surfactants can cause a reverse micelle, which has hydrophobic tails on the outside and the hydrophilic heads interacting with the aqueous layer.[30] Polymerisation takes place within the aqueous core and its size

depends on the size of the micelle. The initiator of the polymerisation was APS, and TEMED, was used to enhance the homolysis of APS.

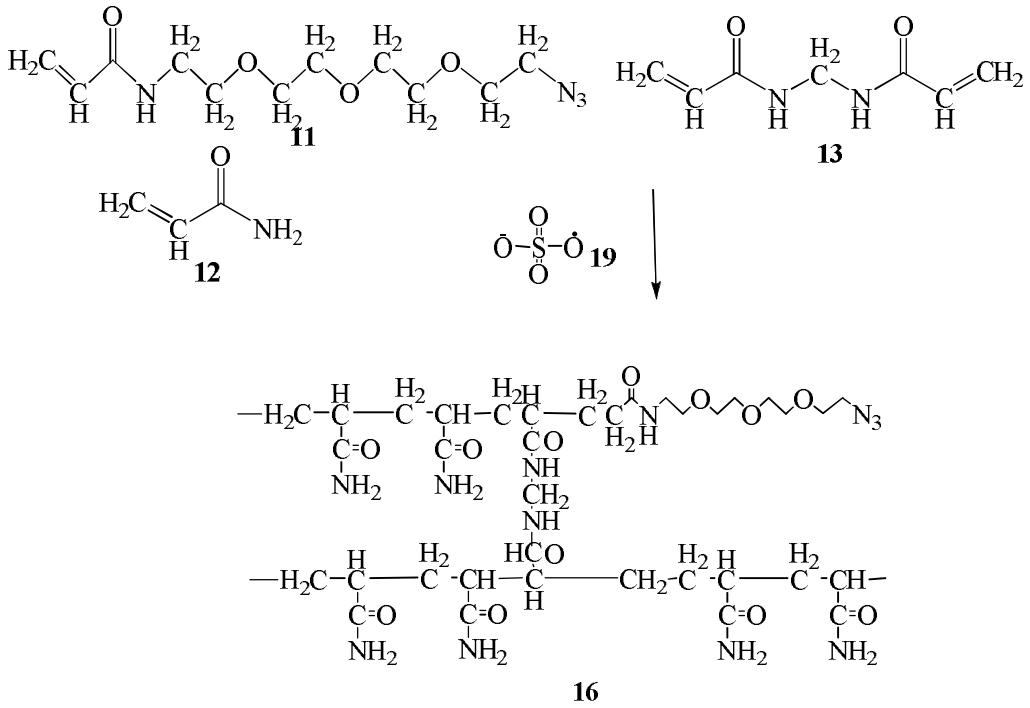

Scheme 2.1.1: Free radical polymerisation of azido bearing nanoparticles.

The free radical polymerisation reaction was allowed to proceed for approximately two hours. Oxygen can act as a terminator for the free radical polymerisation and hence, argon was supplied continuously to avoid any oxygen contamination. The particles were collected by vacuum filtration using a millipore filtration system with a 0.02 µm anodisc filter, as a dried pellet.

2.1.4.1 Characterisation of nanoparticles.

The synthesised, azido bearing nanoparticles were characterised by using FT-IR and DLS analysis.

2.1.4.1.1 DLS analysis

DLS analysis was used to determine the nanoparticle sizes. Water filtered through a 0.2 µm filter was used to prepare 1 mg mL^{-1} solution of the nanoparticles to avoid any dust particles overlap with nanoparticle sizes.

(a) attempt-1 (5.5 %)

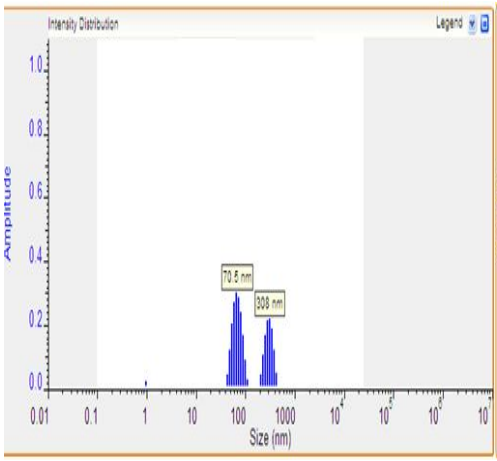

(b) attempt-2 (3.8 %)

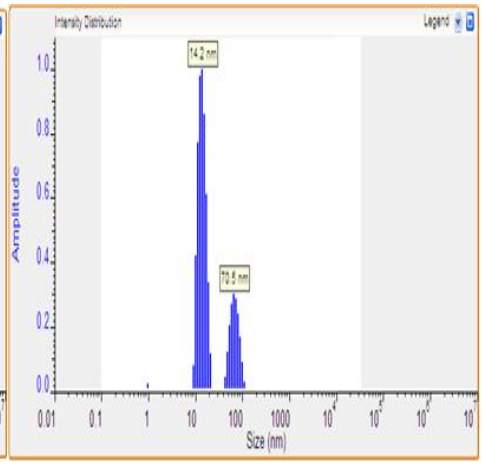

(c) attempt-3 (3.8 %)

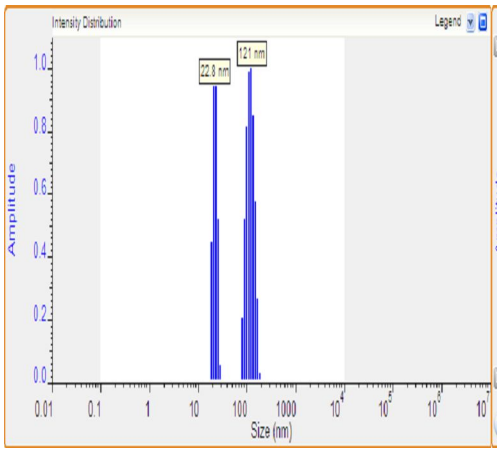

(d) attempt-4 (3.8 %)

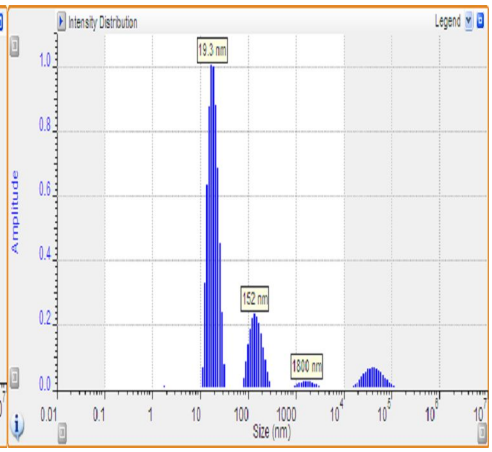

(e) attempt-5 (3.6 %)

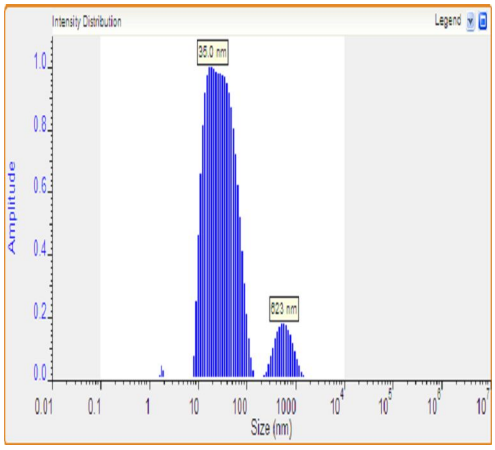

Figure 2.1.3: DLS analysis according to the monomer compositions (Table 2.1.1) (Weight % of azido monomers is shown)

According to the DLS analysis, the optimum particles intensity distributions were obtained at attempt 3 and 4 **(Table 2.1.1)**. When comparing the yields, **(Table 2.1.1)**, and the particle sizes **(Figure 2.1.3)**, the best monomer composition feed of azido bearing nanoparticles was 73.8% of acrylamide **12**, 22.4% of *N*,*N*'methylenebisacrylamide **13** and 3.8% of *N*-(11-azido-3,6,9 trioxaundecanyl) acrylamide **11**.

2.1.4.1.2 FTIR test

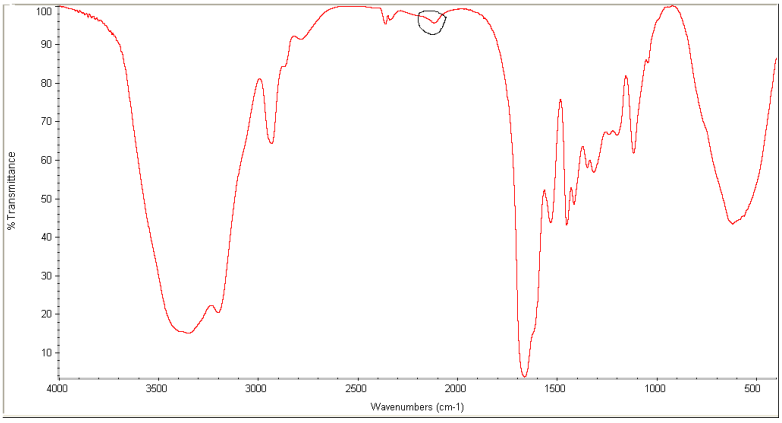

Figure 2.1.4: FT-IR spectrum for azido functionalised nanoparticles.

Dried nanoparticles were characterised by FT-IR. Azido functional group was demonstrated by the appearance of the characteristic transmittance at 2110 cm^{-1} in the FT-IR spectrum (figure 2.1.4).

2.1.5 Availability of the azide functional group

For further confirmation of the presence of the azide functional group, azido functionalised nanoparticles were reacted with alkyne functionalised (5-carboxytetramethylrhodamine) TAMRA dye in the presence of Cu(I) catalyst and the ligand TBTA.[51] The nanoparticles were washed with DMF and ethanol for several times to remove the unreacted reagents. Blank nanoparticles (see section 4.3.1) were also reacted with the alkyne functionalised TAMRA dye using the same conditions (see section 4.4.1)

1 mg mL^{-1} of the above two nanoparticle solutions were excited at λ_{ex} = 555 nm and the success of the CuAAC reaction confirmed by the detection of a noticeable fluorescence signal. Importantly, controls exhibited no significant fluorescence signal (Figure 2.1.5).

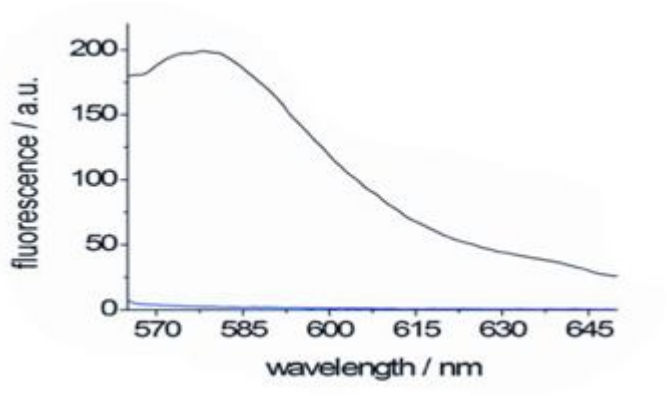

Figure 2.1.5: Emission spectra (λ_{ex} = 555 nm) of alkyne function TAMRA click to azide functionalized nanoparticles.

2.1.6 Application of azido bearing nanoparticles

In addition, exploitation of the azido functionalised nanoparticles, were established by performing a fluorogenic-peptide substrate cleavage reaction (carried out by Dr. Katharina Welser, School of pharmacy, University of Nottingham). Thus, the fluorogenic substrate Z-Gly-Gly-Leu-ACA-Lys (pentynamide)-NH_2 (which was synthesized by Dr. Katharina Welser) was clicked with azido bearing nanoparticles in the presence of Cu(I) catalyst and the ligand TBTA (see section 4.4.2) In this case, the targeted enzyme was subtisilin, which is an enzyme used for studying enzyme-substrate interactions and applied as the model protease for the synthesized substrate. Here, the fluorophore was hetero bifunctional 7-aminocoumarin-4-acetic acid (ACA). These protease targeted peptide substrate bound nanoparticles (1 mg mL^{-1}) were performed in freshly prepared Tris-HCl buffer solution (pH = 8.20) and were incubated at 37˚C for 3 min and treated with different concentrations of subtilisin solution. The fluorescence was monitored for a period of 30 min. (λ_{ex} = 380 nm).

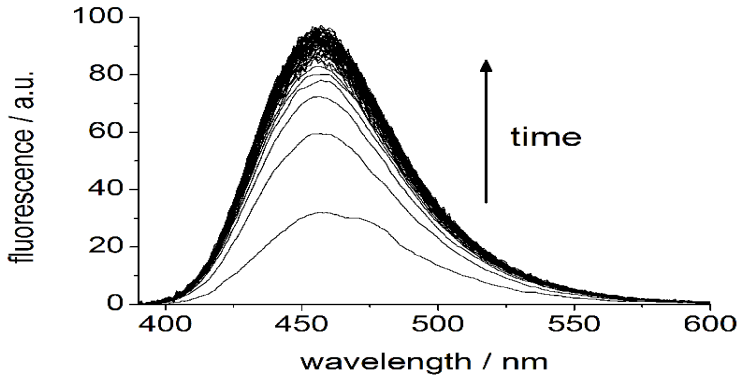

Figure 2.1.6: Subtilisin mediated cleavage reaction of NP clicked (λ_{ex} = 380 nm).

A significant and rapid increase of fluorescence was observed. When the concentration of enzyme was increased under the same conditions, an increase in fluorescence can be seen according to the concentrations (Figure 2.1.6).

2.1.7 Summary

The preparation of azido bearing nanoparticles *via* an inverse microemulsion was readily achieved. The polymerisation reaction was carried out with monomers acrylamide **12**, *N*,*N*'-methylenebisacrylamide **13** and *N*-(11-azido-3,6,9 trioxaundecanyl) acrylamide **11**.

Different compositions of monomer feeds were used to obtain the optimum minimum particle size range of nanoparticles. The composition of acrylamide **11** and *N*,*N*'-methylenebisacrylamide **12** was kept constant and the amount of azido functionalised monomer was changed. According to the DLS analysis, and yields, the best monomer composition feed was 73.8% of acrylamide **12**, 22.4 % of *N*,*N*'-methylenebisacrylamide **13** and 3.8 % of *N*-(11-azido-3,6,9 trioxaundecanyl) acrylamide **11**. The yields were subject to change according to the contamination of atmospheric oxygen which can act as the terminator for the free radical reactions.

The availability of the azido functionalised groups of nanoparticles were checked with the alkynyl-functionalise TAMRA fluorophore and fluorescence was observed from the azide bearing nanoparticles and whilst no fluorescence was observed from the control. The click reaction between alkyne and azide was catalysed by Cu(I) catalyst and was successfully achieved.

In addition, azido bearing nanoparticles were clicked with a protease responsive fluorogenic peptide to measure the substilisin enzyme reactivity and rapid changes of fluorescence confirmed the ability of uses of azido bearing nanoparticles.

2.2 Development of alkyne bearing nanoparticles

2.2.1 Introduction

The aim of this research was to develop and optimize the preparation of nanoparticles bearing alkyne groups. These alkyne bearing nanoparticles could also be modified by the Huisgen Cu(I) catalysed azide-alkyne cycloaddition (CuAAC) reaction.[52] Hence, these nanoparticles can be used to click to other functional chemical groups which contain azide functional groups *via* the CuAAC click reaction.

Propargylamines have been identified as potent anti-apoptotic agents in both *in vitro* and *in vivo* studies. Derivatives of propargylamines have been used to protect neurons against various neurodegenerative disorders.[53] Therefore, the properties of propargylamine can play a vital role in cellular applications of the nanoparticles.

The synthetic strategy of these alkyne functionalised nanoparticles is based on the room temperature microemulsion polymerisation technique, which is known to produce nanometer sized particles with a narrow size distribution.

2.2.2 Types of monomers

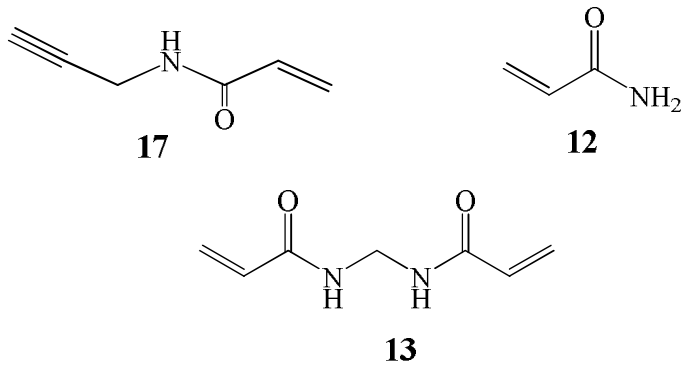

Figure 2.2.1: Monomers used to synthesise alkyne bearing nanoparticles

Three types of monomers were used to synthesise the desired nanoparticles. They are acrylamide **12**, *N,N'*-methylenebisacrylamide **13** and *N*-propargyl acrylamide **17**.

2.2.2.1 Sources of monomers.

Acrylamide and *N*,*N*'-methylenebisacrylamide are commercially available and *N*-propargyl acrylamide **17** was synthesized. Propargylamine **18** and acryloyl chloride **15** were purchased from Sigma Aldrich.

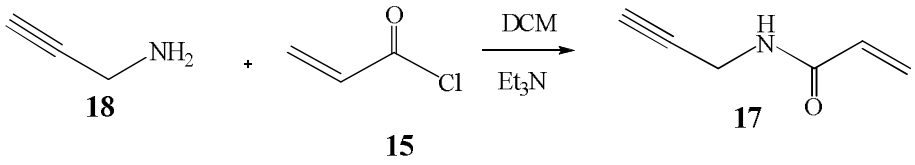

Figure 2.2.2: The acrylation of the alkyne functionalised monomer

The building block *N*-propargyl acrylamide **17** was obtained as a white solid by the reaction of propargylamine and acryloyl chloride (Figure 2.2.2), (see section 4.2.2).

2.2.3 Composition of monomers

During the synthesis, different amounts of *N*-propargyl acrylamide monomer were used within the range of 2.0 % and 4.1 % of the total monomer amount. The amount of acrylamide **12** and *N*,*N*'-methylenebisacrylamide **13** were kept constant to obtain nanometer range particles.

Table 2.2.1: The monomer compositions of alkyne bearing nanoparticles, synthesised by using different ratio of reactants and reacted for 2 hours.

Attempt	Amount of monomers (mg)				Recovered yield (mg)
	Alkyne	Acrylamide	Bisacrylamide	Expected yield	
1	9.0 (2.5%)	265	80	354	239.0
2	7.0 (2.0%)	265	80	352	226.5
3	15.0 (4.1 %)	265	80	360	188.3
4	13.0 (3.6%)	265	80	358	207.8
5	12.0 (3.4%)	265	80	357	259.0
6	12.0 (3.4%)	265	80	357	155.0

The polymerisation procedure of the alkyne bearing nanoparticles was similar to the azido bearing nanoparticles (see section 4.3.3).

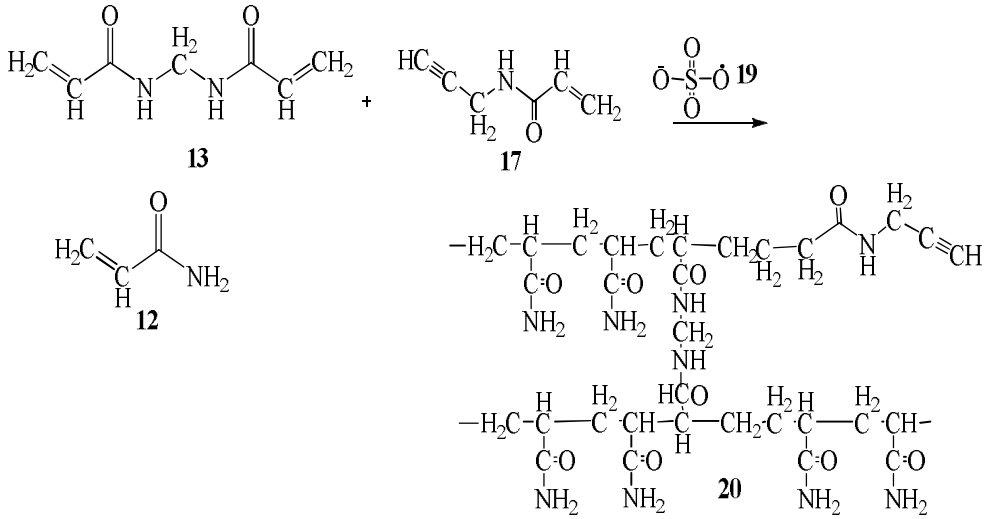

Scheme 2.2.1: Free radical polymerisation of monomers of alkyne bearing of nanoparticles.

In the polymerisation mixture, APS **19** acts as the free radical initiator to form acrylamide free radicals. These activated acrylamides react with other acrylamide **12** and *N*-propargyl acrylamide **17** to form liner polymer chains. *N,N'*-methylenebisacrylamide **13** crosslinks these chains (Scheme 2.2.1).

2.2.4. Characterisation of nanoparticles.

2.2.4.1. FT-IR

FT-IR was used to characterise the alkyne bearing nanoparticles (figure 2.3.3). A broad peak (3600 cm^{-1} to 2900 cm^{-1}) was observed, which corresponded to the NH and backbone of the nanoparticles. The peak for the carbonyl carbon of the monomers was obtained at 1661 cm^{-1} and the sharp peak related to the alkyne group (alkyne C-H) of the *N*-propargyl acrylamide monomer was expected at around 3300 cm^{-1} and but was masked by the backbone of nanoparticles related broad peak and was not enough to prove the availability of the alkyne group.

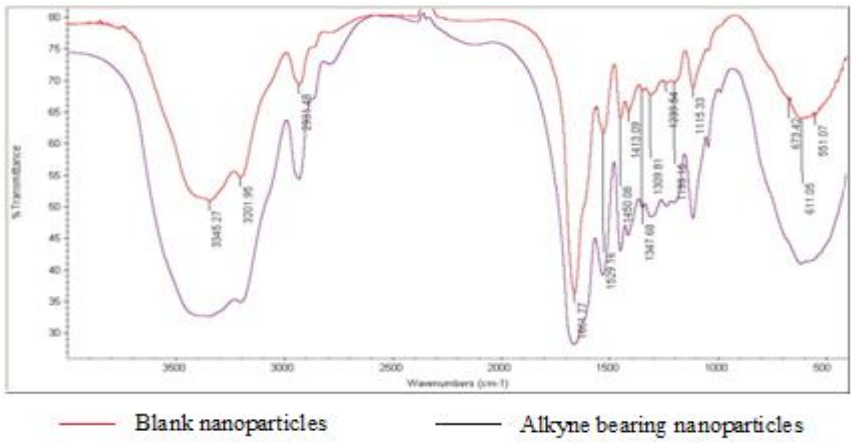

Figure 2.2.3: FTIR spectra for alkyne functionalised nanoparticles.

2.2.4.2 DLS analysis

DLS analysis was carried out the nanoparticles to demonstrate their particle sizes. Normally, particle sizes of polyacrylamide matrices should be obtained which are less than 100 nm in radius and larger sizes were considered due to aggregation of the droplets of water joining into successively larger formations, which subsequently polymerised. When the sizes were larger, they were filtered through the 0.2 µm filter to remove them from the sample

(a) attempt-1 (2.5 %) (b) attempt-2 (2.0 %)

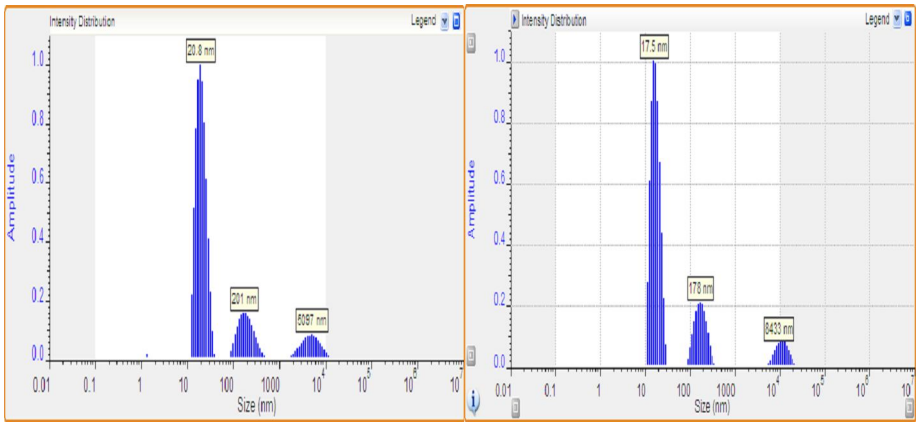

(c) attempt-3 (4.1 %) (d) attempt-4 (3.6 %)

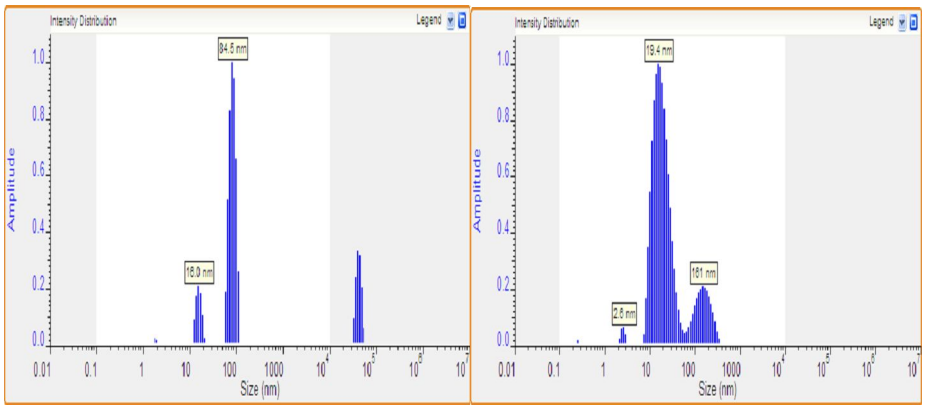

(e) attempt-5 (3.4%) (f) attempt-6 (3.4%)

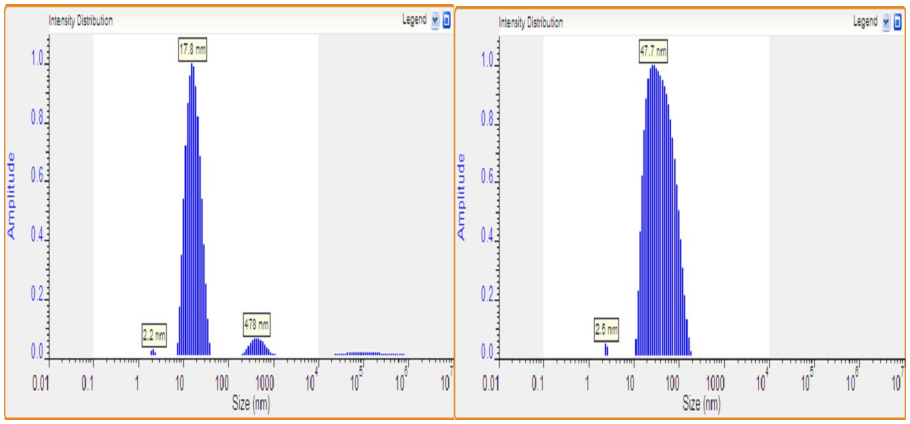

Figure 2.2.4: DLS analysis according to the monomer compositions. (Table 2.1.1) (Weight % of alkyne monomers is shown above).

When comparing the yields, (Table 2.2.1) and the particle sizes (Figure 2.2.4) the best monomer composition feed of alkyne bearing nanoparticle was 74.4

% of acrylamide, 22.4 % of *N*,*N*'-methylenebisacrylamide and 3.4 % of *N*-propargyl acrylamide.

2.2.5 Availability of the alkyne functional group

FT-IR analysis failed to confirm the presence of the alkyne group. Therefore, the availability of the alkyne functional group was doubtful. To confirm the availability of alkyne group, azide functionalised fluorophore was clicked (Figure 2.2.5) *via* CuAAC click reaction[51] (see section 4.5.1). The click reaction conditions were similar to the previously mentioned click reaction of azido bearing nanoparticles (see section 2.1.5). A control was also carried out with blank nanoparticles.

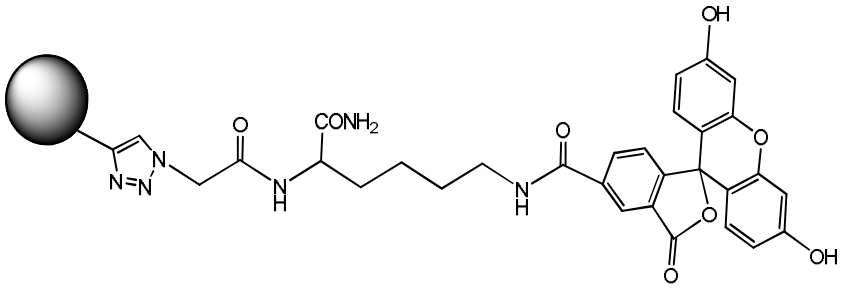

Figure 2.2.5: Azido functionalised fluorophore clicked to alkyne functionalised NP.

The fluorophore conjugated alkyne nanoparticles and controls were suspended in aqueous (1 mg mL^{-1}) solution. The alkyne bearing nanoparticles exhibited noticeable fluorescence (Figure 2.2.6) and most importantly, the control exhibited no fluorescence.

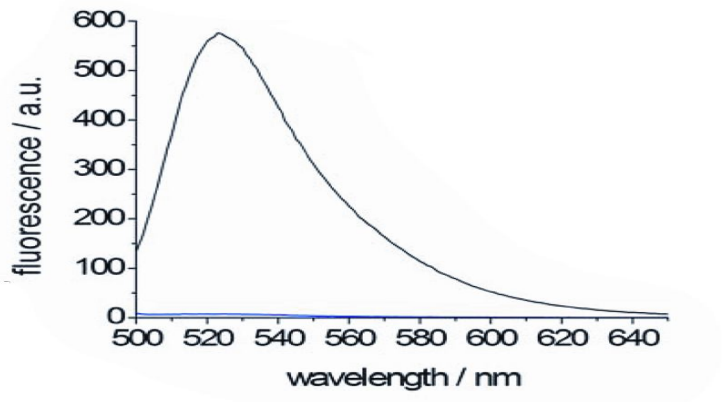

Figure 2.2.6: Emission spectra (λ_{ex} = 490 nm) of alkyne functional nanoparticle clicked to azide functionalised fluorescence peptide

2.2.6 Application of alkyne nanoparticles

Alkyne bearing nanoparticles were prepared for ratiometric pH response (carried out by Dr. Katharina Welser, School of pharmacy, University of Nottingham). TAMRA dye conjugated with dextran (to prevent the leaching of TAMRA dye) was incorporated with alkyne bearing nanoparticles in the inverse microemulsion (see section 4.3.6). The nanoparticles were then clicked to pH sensitive azido functionalised 5-carboxyfluorescein (5-FAM) fluorophore (see section 4.5.1). Using phosphate buffer saline (PBS), solutions of pH range 5.3 to 7.6 were prepared. Then 1 mg mL^{-1} of solution of each nanoparticle was prepared for each pH solution and fluorescence was observed (Figure 2.2.7). 5-FAM and TAMRA dyes were excited at 490 nm and 555 nm and emission was recorded at 520 nm and 580 nm respectively. The TAMRA dye has been used as the standard. Fluorescence was observed according to the pH of the solutions (Figure 2.2.7).

.

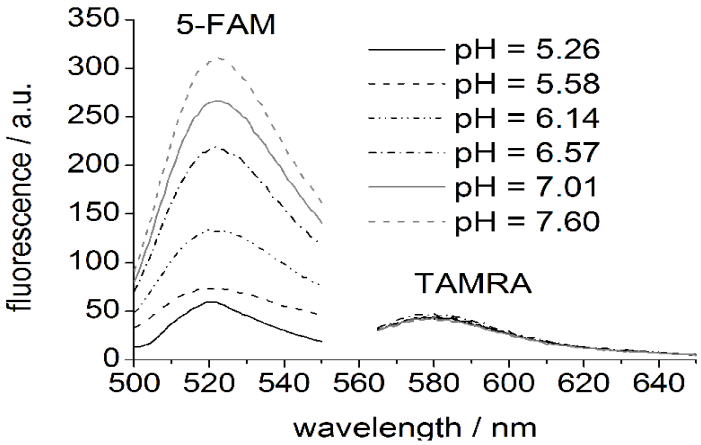

.

Figure 2.2.7: Emission spectra of pH-responsive nanoparticles observed at different pH values (λ_{ex} = 490 nm 5-FAM and 555 nm for TAMRA).

2.2.7 Summary

This chapter discussed the preparation of alkyne bearing nanoparticles and polymerisation reactions were carried out with the monomers acrylamide **11**, *N*,*N*'-methylenebisacrylamide **12** and *N*-propargyl acrylamide **17**.

The presence of the alkyne bearing nanoparticles in the reaction mixture was checked with the azide bearing 5-carboxyfluorescein and a positive outcome was observed, while no fluorescence was observed from the control. FT-IR analysis failed to show a positive verification of alkyne groups and related IR peaks (both alkyne C-C and C-H) were masked in the polyacrylamide backbone related broad peaks.

In addition, alkyne bearing TAMRA conjugated nanoparticles were clicked to a pH responsive fluorophore and the different fluorescent signals according to the pH values of solvents were observed.

2.3. Development of maleimide bearing nanoparticles

2.3.1 Introduction

The aim of the research was to develop and optimise the preparation of nanoparticles bearing maleimide groups and then check the availability of the maleimido functional group.

Maleimide functional groups have an alkene group and can be modified with the thiol-alkene click reaction at room temperature.[54] Normally, thiol-maleimide click reactions occur faster than most of the other nucleophilic reactions with maleimides.[40]

Maleimide containing compounds can act as linkers.[55,56] They are readily available and are very useful tools in bioconjugate chemistry. Maleimide derivatives include various shares among immobilized antibodies, enzymes and peptide conjugate derivatives.[56] These maleimide molecules, with their vinyl group, are very reactive and are capable of participating in various reactions such as nucleophilic additions and Diels Alder reactions[57].

2.3.2 Types of monomers

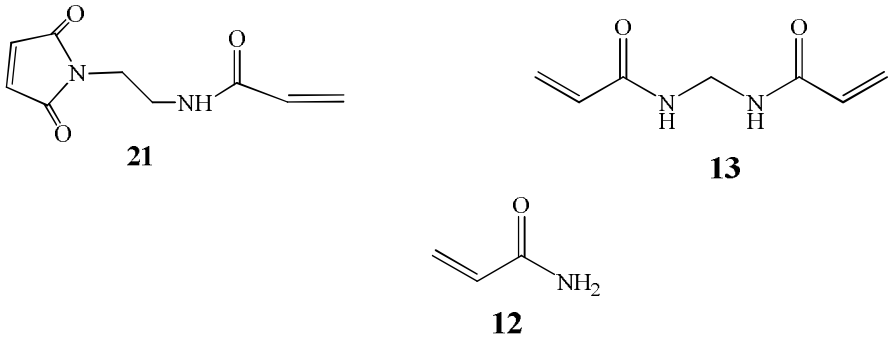

Figure 2.3.1: Monomers used to synthesise maleimide bearing nanoparticles.

Three types of monomers were used to synthesise maleimide bearing nanoparticles. They were acrylamide **12**, *N*,*N*'-methylenebisacrylamide **13** and *N*-(maleimidoethyl) acrylamide **21.**

2.3.3 Sources of monomers.

N-(maleimidoethyl) acrylamide **21** was synthesized in the laboratory. (Figure 2.3.5). The maleimide building block **21** was obtained by the reaction of 1-(2-aminoethyl)-1H-pyrrole-2,5-dione salt (see section 4.2.4.2) **22** and acryloyl chloride **15**.

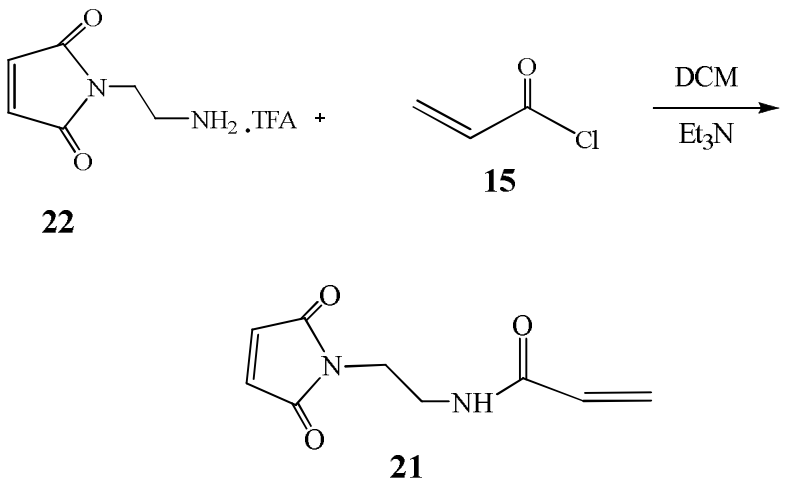

Figure 2.3.2: The acrylation reaction of the maleimide functionalised monomer.

The desired product **21** was found to display aqueous solubility. Therefore, reaction mixture was separated directly using the column chromatography (hexane: EtOAc= 1:1), without washings.

2.3.3.1 Attempt of synthesis of 1-(2-aminoethyl)-1H-pyrrole-2, 5-dione (22) using Mitsunobu reaction conditions.

The Mitsunobu[58-60] reaction is one of the most useful and specific reactions in organic chemistry due to its versatility and effectiveness.[58] The beauty of this reaction is that it converts primary or secondary alcohols into an excellent leaving group which can be displaced with a wide range of nucleophiles either intra or inter molecularly and can be categorized as modern SN^2 reaction.[59] This reaction has a complex mechanism and involves the reaction between an alcohol and an acidic nucleophile in the presence of triphenylphosphine and azodicarboxylate or azodicarboxamide. There have been some debates around identifying its intermediate compounds and the roles they play.[60] In the first step, triphenylphosphine and diisopropyl azodicarboxylate (DIAD) react to form a betaine intermediate **29**. [61]

Under the Mistunobu conditions, maleimide **25** acts as the acidic nucleophile. The primary alcohol of *tert*-butyl 2-hydroxyethylcarbamate **24** was converted into an excellent leaving group. Free amino group of 2-aminoethanol **23** had to be masked to avoid the unnecessary reactions with intermediates of the Mitsunobu reaction. Therefore, the amine functional group was first temporary protected by a Boc protecting group[62-65] (Figure 2.3.3).

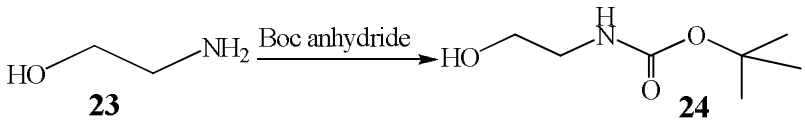

Figure 2.3.3 Boc protection of 2-aminoethanol **23.**

Boc anhydride was treated with 2-aminoethanol **23** in DCM (see section 4.2.3.1). The crude product, dissolved in ethyl acetate, was washed with aqueous acid (pH=4) to remove the unreacted 2-aminoethanol **23**.

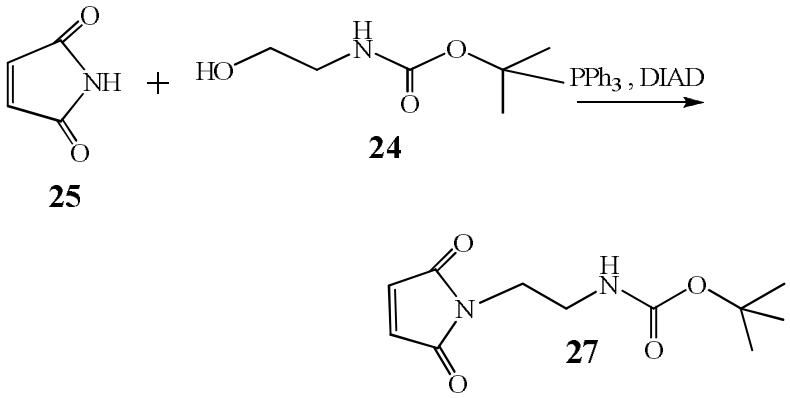

Figure 2.3.4: synthesis of *tert*-butyl 2-(2,5-dioxo-2H-pyrrol-1(5H)-yl)ethylcarbamate **27.**

The tert-butyl 2-hydroxyethylcarbamate **24** and maleimide **25** were reacted in the presence of triphenyl phosphine (PPh_3) and diisopropyl azodicarboxylate (DIAD) in anhydrous tetrahydrofuran (THF) (see section 4.2.3.2).

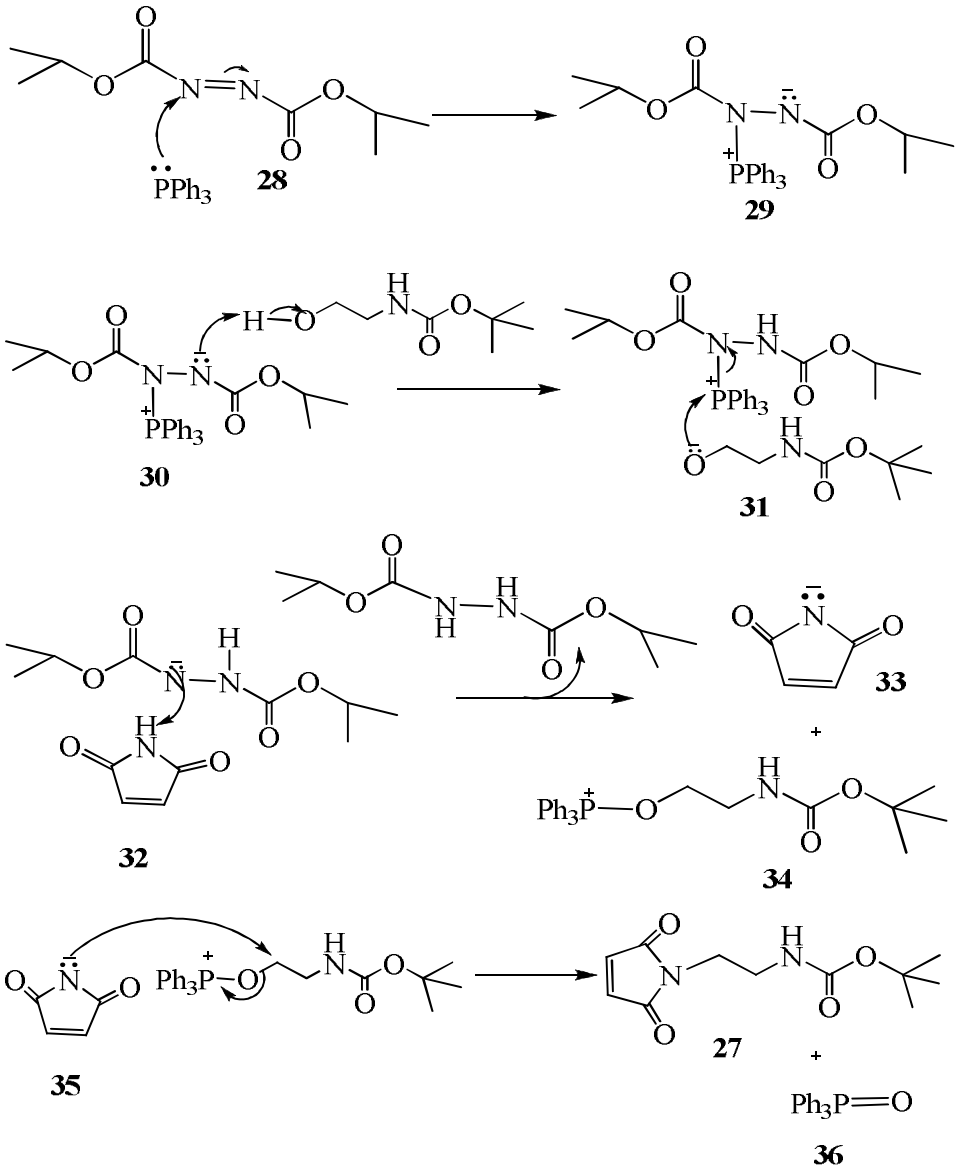

Figure 2.3.5 Mechanism of the Mitsunobu reaction. [59, 61, 66]

Initially, PPh_3 makes a nucleophilic attack on to the DIAD and creates the betaine intermediate **29**.[59] Unpaired electrons on the negatively charged nitrogen of the betaine intermediate **29** deprotonate the OH group of the *tert*-butyl-2-hydroxyethylcarbamate **30** to form a negatively charged *tert*-butyl 2-hydroxyethylcarbamate ion. The deprotonated negatively charged alkoxide then nucleophilically attacks the electrophilic phosphorus centre of the betaine and forms the key oxophosphonium intermediate **34**. Simultaneously, the negatively charged unpaired electrons of nitrogen of the betaine intermediate, nucleophilically attacks and deprotonates maleimide **32**. The deprotonated maleimide then nucleophilically attacks the oxophosphonium intermediate **35**

and produced the desired product **27** and the phosphine oxide **36** as the co-product.[59]

The solvent was evaporated and the residue was triturated with diethyl ether to remove the co-product **36** from the crude product. Thin layer chromatography (TLC) analysis of the crude product showed several spots in addition to the starting materials. To purify the crude product, column chromatography was done and each fraction was analysed with ^{1}H NMR and mass spectrometry. The desired product was absent and the major isolated product was maleimide **25** as a white solid, which was approximately 85 % of the initially added amount. Therefore, an alternative synthetic approach was considered to produce the 1-(2-aminoethyl)-1H-pyrrole-2,5-dione **22.**

2.3.3.2 The alternative approach of synthesising 1-(2-aminoethyl)-1H-pyrrole-2,5-dione (22)

Maleic anhydride **37** has an anhydride group and ring opening of it occurs with the nucleophilic attack of amine on to the carbonyl carbon. The reaction between amine and carbonyl carbon initially makes an amide bond. Nucleophilic attack of the nitrogen of the amide bond makes the ring close and produces maleimides.[67]

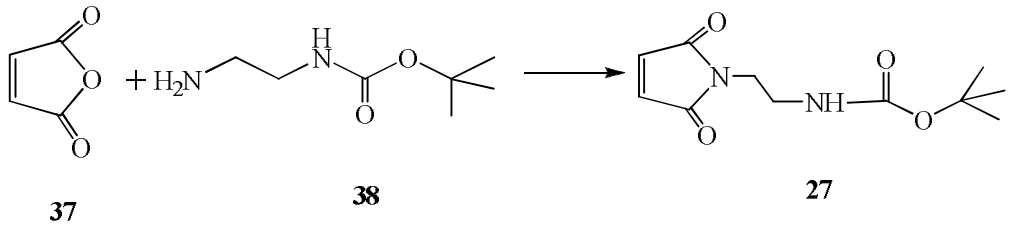

37 **38** **27**

Figure 2.3.6: Addition of maleic anhydride to the *tert*-butyl 2-aminoethylcarbamate. [68]

Tert-butyl 2-aminoethylcarbamate **38** and maleic anhydride **37** were reacted in the presence of diisoprophylethylamine (DIPEA) in diethyl ether (chapter 4.2.4.1). During the reaction, *tert*-butyl 2-aminoethylcarbamate nulceophilically attacks the carbonyl carbon of the anhydride **39** group of the maleic anhydride and open its ring **40**. DIPEA was added to form a carboxylate anion and TBTU makes the ester bond with the carboxylate anion to make a

good leaving group **45**. Then the nitrogen of the amide bond nucleophilically attacks the carbonyl carbon of the ester bond to make the desired product **27**.

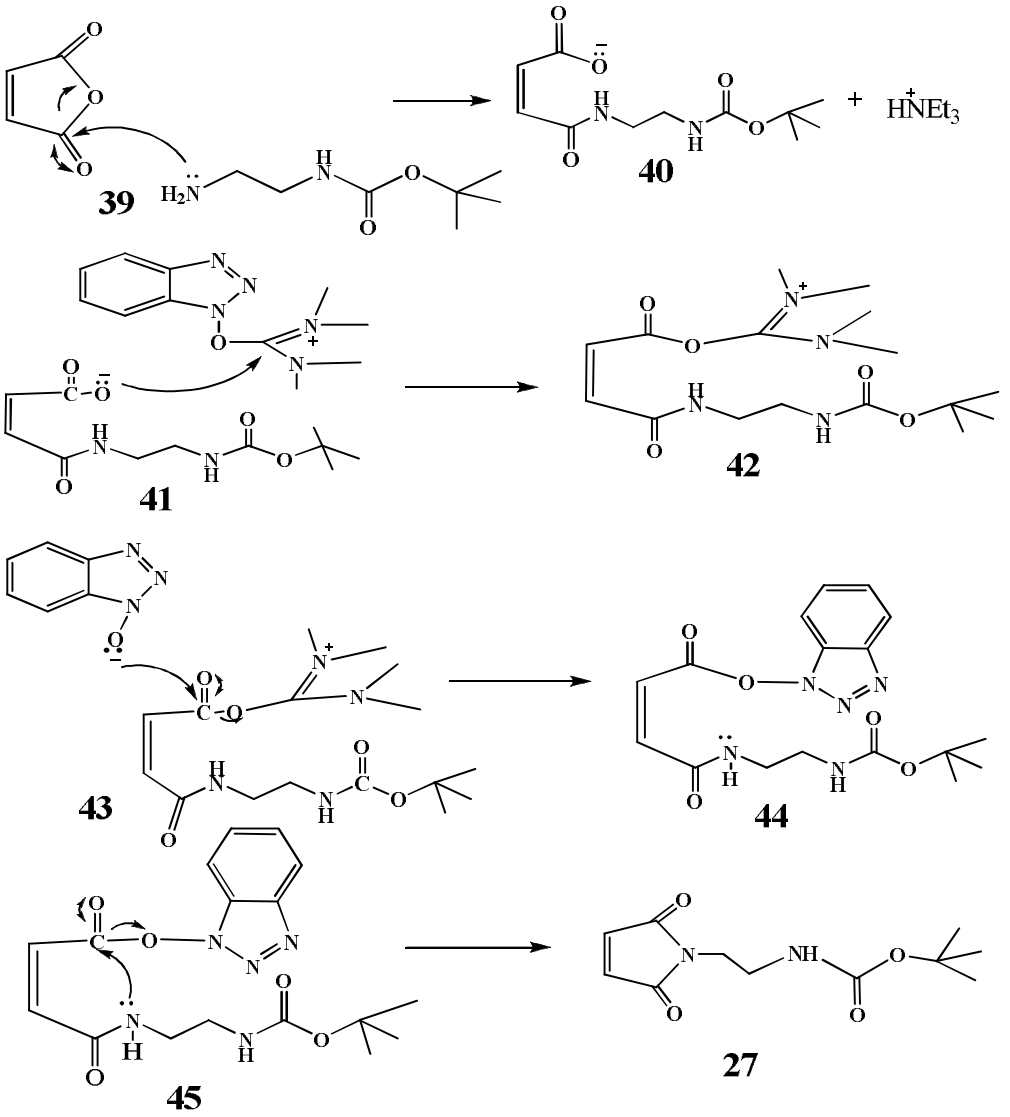

Scheme 2.3.1: Mechanism of addition of the maleic anhydride to the *tert*-butyl 2-aminoethylcarbamate.[68]

The *tert*-butyl 2-(2,5-dioxo-2H-pyrrol-1(5H)-yl)ethylcarbamate **27** was then deprotected with trifluoroacetic acid (TFA) and the resulted product **22,** was reacted with acryloyl chloride **15** to obtain the maleimide building block **21** (Figure 2.3.2).

2.3.4 Composition of monomers

All the amount of acrylamide **12**, *N*,*N*'-methylenebisacrylamide **13** were kept constant and amount of maleimide monomer was changed.

Table 2.3.1: The monomer compositions of maleimide bearing nanoparticles, synthesised by using different ratio of reactants and reacted for 2 hours.

Attempt	amount of monomers (mg)				Recovered yield (mg)
	Maleimide	Acrylamide	Bisacrylamide	Expected yield	
1	10 (2.8%)	265	80	355	244.6
2	12 (3.3%)	265	80	357	56.5
3	25 (6.7%)	265	80	370	221.8
4	20 (5.4%)	265	80	365	181.7
5	15 (4.1%)	265	80	360	178.0

Due to oxygen contamination, the yield of attempt 2 was decreased. Here, the oxygen can act as the terminator for the free radical reaction. The highest yield is given by the lowest amount of maleimide monomer (Table 2.3.1). Synthesised maleimide bearing nanoparticles were characterised by using DLS and FT-IR analysis.

(a) attempt-1 (2.8%) (b) attempt-2 (3.3%)

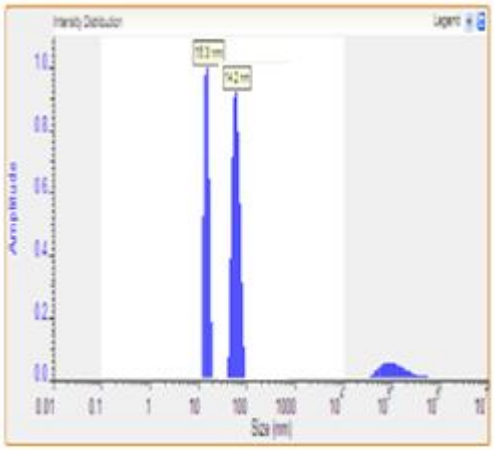

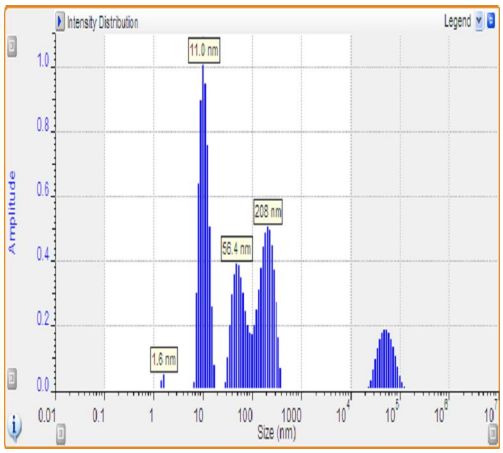

(c) attempt-3 (6.7 %) (d) attempt-4 (5.4 %)

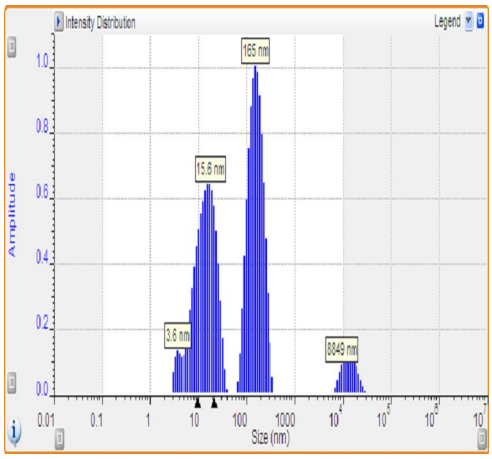

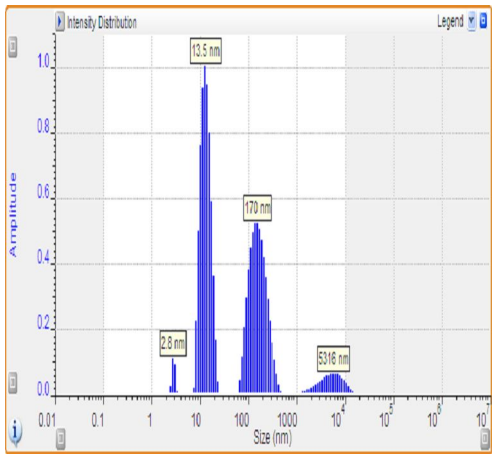

(e) attempt-5 (4.1 %)

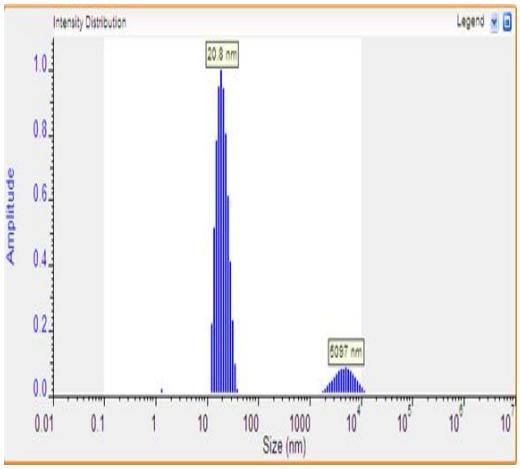

Figure 2.3.7: DLS analysis according to the monomer compositions of maleimido bearing nanoparticles (Weight % of maleimide monomers is shown).

DLS analysis results (figure 2.3.7) show that optimum particle intensity distributions were obtained in attempt 1 and 5. When comparing both yield and the particle sizes together, the best monomer composition feed was 74.6 % of acrylamide **12**, 22.6 % of *N,N'*-methylenebisacrylamide **13** and 2.8% of *N*-(maleimidoethyl) acrylamide **21**.

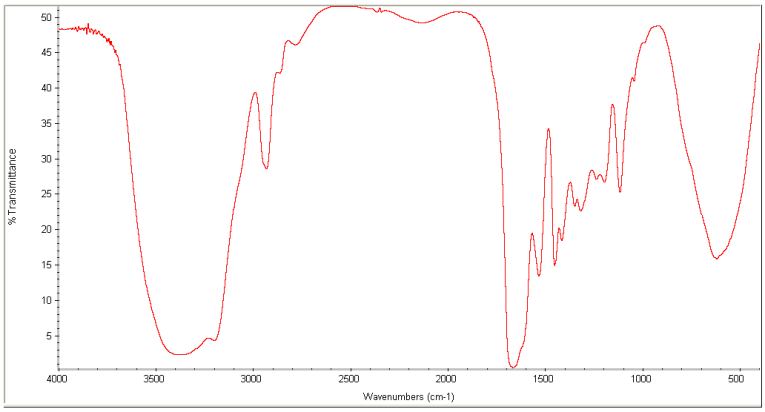

Figure 2.3.8: FTIR spectra for maleimide functionalised nanoparticles.

According to FT-IR, the carbonyl carbon of the monomers was identified at 1671 cm^{-1}. The peaks relating to the alkene functional group of the N-(maleimidoethyl) acrylamide **21** were expected to appear at 3100 cm^{-1} and 1591 cm^{-1} but were masked by the broad peaks of nanoparticle backbone.

2.3.6 Availability of the maleimide functional group of the nanoparticles.

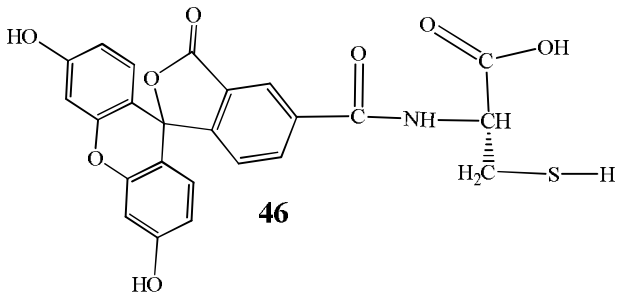

46

Figure 2.3.9: Cysteine modified 5-carboxyfluorescein fluorophore.

The availability of the maleimide was checked with the maleimide-thiol click reaction with thiol containing cysteine modified 5-carboxyfluorescein fluorophore **46** (which was synthesised by Dr. Cillian Byrne, School of pharmacy, University of Nottingham). A control reaction which was identical

in conditions, except that unmodified nanoparticles were used, was carried out. (see section 4.6)

Full availability of maleimide functional groups in the nanoparticles was doubtful. The alkene bond of maleimide molecule can undergo reaction during the free radical polymerisation[69] and can act as the bifunctional linkers in the polymerisation.

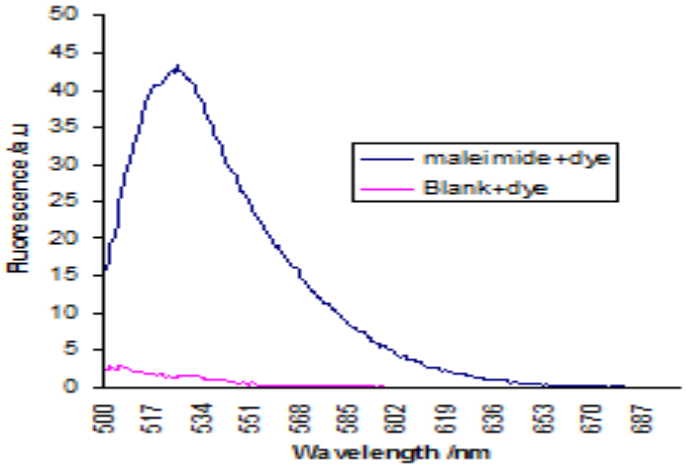

Figure 2.3.10: Emission spectra (λ_{ex} = 490 nm) of cysteine modified carboxyfluorescein click to maleimide functionalized nanoparticles.

However, significant fluorescence was obtained only from the cysteine modified carboxyfluorescein clicked nanoparticles (Figure 2.3.10) which confirmed that the maleimide alkene functional groups are still available.

2.3.6.1 Calculation of remaining maleimide functional groups in nanoparticles

Maleimide functional groups can be involved in the free radical polymerisation and availability of the free maleimide functional groups was calculated according to the fluorescence of 1 mg mL^{-1} of the sample. (See section 4.8). Known concentrations of cysteine modified carboxyfluorescein solution series were prepared and their maximum fluorescence was measured (See section 4.8).

2.3.7 Summary

The optimum monomer composition feed was 74.6 % of acrylamide **12**, 22.3 % of *N*,*N*'-methylenebisacrylamide **13** and 2.8 % of *N*-(maleimidoethyl) acrylamide **21**.

To synthesise, 1-(2-aminoethyl)-1H-pyrrole-2,5-dione **22** two synthetic methods were used and the reaction similar to Mitsunobu condition, failed. Therefore, an alternative pathway, the addition of the maleic anhydride to the *tert*-butyl 2-aminoethylcarbamate **38**, reaction was successfully followed affording the desired product **22**. The addition of the maleic anhydride to the *tert*-butyl 2-aminoethylcarbamate approach yielded 36 % of the purified product **22** and Van Der Veken and co-workers[67] have already synthesised product **22** using the same conditions (see section 4.2.4.1) and had obtained the yield of 38 %.

Maleimide functionalised monomer has two alkene group on its structure and both can be involved in the free radical polymerisation reaction. The maleimide functional group was clicked with cysteine modified carboxyfluorophore **46** to check the availability and the result was positive. However 99.3 % of the maleimide (see section 4.8.2) monomers have been involved in free radical polymerisation reaction and only 0.7 % of the maleimide functional groups are available (see section 4.8.2).

Chapter 3

3.0 Conclusions and future work

Polyacrylamide matrices can be synthesised to obtain various functional groups when monomers containing alkene bonds are used in free radical polymerisation. In this research, three types of monomers containing different functional groups were used to synthesise nanosize particles by free radical polymerisation.

All these polymerisations were carried using an inverse microemulsion and argon was supplied continuously to prevent the oxygen contamination. Oxygen can act as an inhibitor of the free radicals and can directly affect the yield of the product. All the time, acylamide **12** and *N*,*N*'-methylene bisacrylamide monomers **13** were kept constant to obtain nanoscale nanoparticles and only the functional monomer amount was changed. The optimum monomer feed was obtained for each type of monomer according to the DLS analysis. NMR technique did not work on polymerised nanoparticles and was unable to characterise nanoparticles with NMR analysis.

3.1 Azido and alkyne functionalised nanoparticles

According to the DLS analysis, 3.8 % of *N*-(11-azido-3,6,9-trioxaundecanyl) acrylamide monomer was the best composition of monomer feed to carry out the future azido bearing nanoparticle polymerisation reactions and the observed average particle size was 22.8 nm in diameter (Figure 3.1).

Alkyne bearing nanoparticles having 3.4 % of the *N*-propargyl acrylamide building block was the best composition of monomer feed to carry out the polymerisation and the observed average particle size was 17.8 nm in diameter (Figure 3.1). In both polymerisations, obtained particle sizes were the desired sizes for the biological applications.

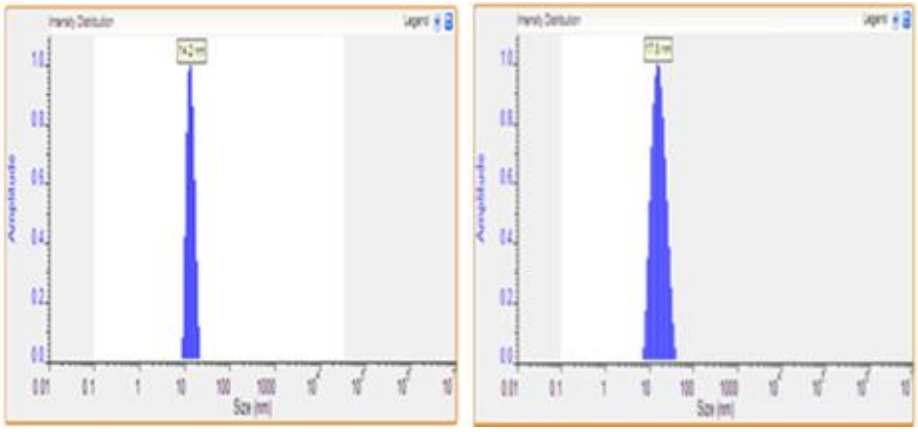

(a) (b)

Figure 3.1: Nanoparticles, filtered with 0.2 μm filters. (a) azido bearing nanoparticles (b) Alkyne bearing nanoparticles.

The dyes (cysteine modified 5-carboxyfluorescein fluorophore and TAMRA fluorophore) loading of azido and alkyne functionalised monomers were 0.13 and 0.30 μmol mg^{-1} respectively and were enough to detect a fluorescence signal. The TAMRA fluorophore and 5-carboxyfluorescein were excited respectively at $\lambda_{ex=}$ 555 nm and at λ_{ex}= 490 nm and availability of azido and alkyne functional groups were precisely confirmed by the detection of a noticeable fluorescence signal and importantly, the control exhibited no fluorescence. Therefore, none of the fluorophore was physically adsorbed with nanoparticles.

In addition to observing the conjugation capacity, fluorogenic substrate containing protease targeted peptide was clicked with azido bearing nanoparticles and fluorescence was observed for different enzyme concentrations. The fluorescence changed rapidly according to the enzyme concentrations and the results were promising.

To illustrate the conjugation capacity of the clickable nanoparticles, TAMRA-dextran conjugated nanoparticles were clicked with pH sensitive 5-carboxyfluorescein. Dextran was bound to TAMRA to prevent the leaching from nanoparticles and used as the reference fluorophore. These nanoparticles emitted different fluorescent signals depending on the pH of the solutions and were able to measure the unknown pH of water sample successfully.

3.2 Maleimide functionalised nanoparticles

According to the DLS measurements 74.6% of acrylamide **12**, 22.6% *N,N'*-methylene bisacrylamide **13** and 2.8 % monomer composition was the best composition of monomer feed to carry out the polymerisation and the observed average particle sizes were 20.8 nm in diameter (Figure 3.2), which was the desired size for the biological applications.

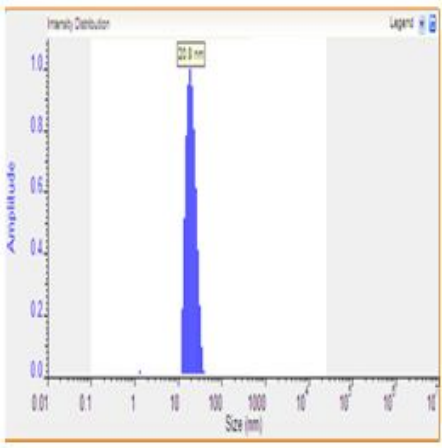

Figure 3.2: Maleimido nanoparticles filtered with 0.2 µm filters.

The nanoparticles-clicked dye loading was 0.14 µmol/mg of nanoparticle, which was enough to obtain fluorescence. The success of the thiol-maleimide reaction was confirmed by the fluorescence signal when the nanoparticle suspension was excited at λ_{ex} 490 nm. The absence of fluorescence from the control indicated that click reaction thiol-maleimide was successful and not just physically adsorbed.

The intensity of fluorescence observed from the nanoparticle suspension was compared with the freshly prepared known concentrations of fluorophore solutions and concentration of the maleimide in 1 mg mL^{-1} of nanoparticles was identified. According to the calculations, 99.3% of the maleimide functional alkene groups were involved in the polymerisation. However, less than 1% was available for the click reaction and for further modifications.

3.3 Future work

To prevent the maleimide moiety of the functional monomers to be involved in the free radical polymerisation reaction and hence enhance the availability of these functional groups in the final materials, they will be masked during polymerisation.

Overall, future work can be divided into two main sections.

- Temporary protection of the maleimide functional group.
- Synthesis of vinyl ester-bearing nanoparticles

3.3.1 Temporary protection of the activity of the maleimide functional group.

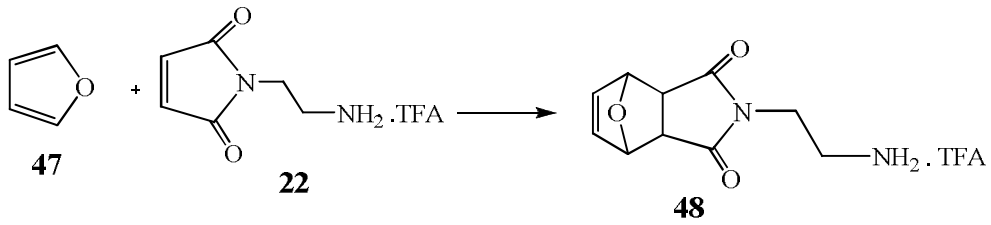

Figure 3.3: Protection of the maleimide double bond.

The protection of the maleimide double bond can be accomplished through a Diels-Alder reaction using furan **47** as a diene and 1-(2-aminoethyl)-1H-pyrrole-2, 5-dione **22** as a dienophile (figure 3.3).

Once polymerisation is completed, the reaction mixture will be heated for 1 hour at reflux temperature of anisole (retro Diels-Alder step), affording the desired deprotected maleimide product.[66] This method will increase the availability of the maleimide functional groups of the nanoparticles

3.3.2 Synthesis of vinyl ester bearing nanoparticles.

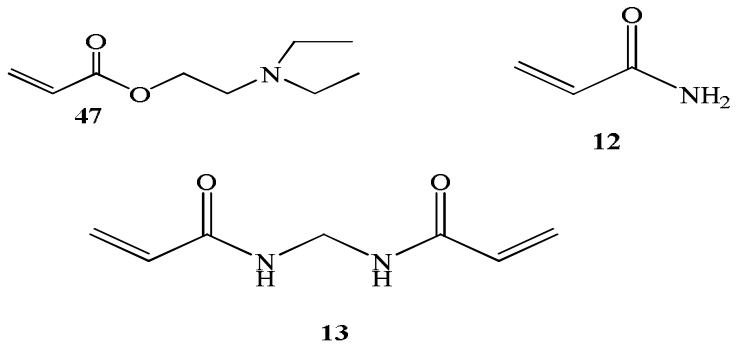

Figure 3.4: Monomers employed for the synthesis of vinyl ester-containing nanoparticles.

Acrylamide **12**, *N,N'*-methylenebisacrylamide **13** and 2-(diethylamino)-ethyl acrylate **47** were the three types of monomers which were involved in the polymerisation. All the monomers, including 2-(diethylamino)-ethyl acrylate **47** are commercially available and will be used to prepare the 2-(diethylamino)-ethyl acrylate containing nanoparticles **50**.

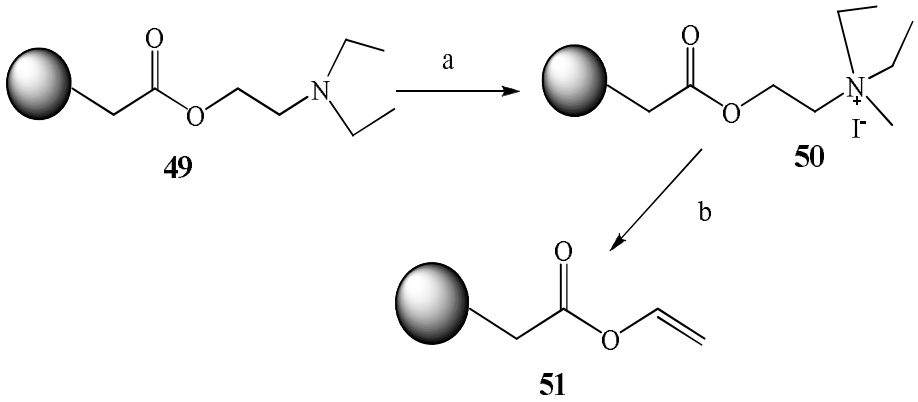

Figure 3.5: (a) Methylation of nanoparticles tertiary amine groups (b) Hofmann elimination.

2-(Diethylamino)-ethyl acrylate contained in nanoparticles **49** will be converted in to the vinyl esters **51**. The nanoparticles **49** will be treated with excess MeI in DMF solution, converting the tertiary amine of nanoparticles **49** into quaternary ammonium salts in **50**. The quaternised nanoparticles will then be treated under Hofmann elimination reaction conditions.[70-72] As a result tertiary amine is released as the co-product and finally, vinyl ester nanoparticles **51** will be formed. The availability of the vinyl ester bearing nanoparticles can be checked with the thiol-bearing 5-carboxylflurescein **46** *via* a vinyl ester thiol click reaction.

Chapter 4

EXPERIMENTAL

4.1 Materials and Instruments

Chemicals and solvents were purchased from Sigma Aldrich and used without further purification. Deuterated solvents for NMR tests were purchased also from Sigma Aldrich. Dichloromethane and diethyl ether were dried over molecular sieves. For chemical reactions, nanoparticle synthesis and analysis, milli-Q water was used. Reactions were monitored by analytical thin-layer chromatography (TLC) on commercially available precoated aluminium plates (Merck Kieselgel 60 F_{254}) and screening of TLC plates was done using a UV lamp (λ_{max} = 254 nm) and freshly prepared potassium permanganate staining.

Using Nicolet IR 200 FT-IR spectrophotometer in the range of 4000–500 cm^{-1} using KBr and NaCl discs, infrared spectra were recorded. Transmitance maxima (υ_{max}) are reported in wave-numbers (cm^{-1}) and classified as strong (s), medium (m) or broad (br).

The Waters 2795 separation module/micromass LCT platform mass spectra (TOF-ES) were used to analyse by mass spectrometry. Organic solvents were evaporated using a rotary evaporator under reduced pressure at room temperature.

Melting points were monitored on a Gallenkamp melting point apparatus. Sizes of the nanoparticles were observed by dynamic light scattering (DLS) using a Viscotec Model 802 instrument equipped with an internal laser (825-832 nm) with a maximum radiation power of 60 mW. Data processing was performed with the software program OmniSize3.

^{1}H NMR resonance (δ^{H}) and ^{13}C NMR (δ^{C}) spectra were recorded at 20 °C on a Bruker Avance-400 instrument operating at 400 MHz and 100 MHz. Chemical shifts (δ) are reported in parts per million (ppm), reference to deuterated solvents. The coupling constants *J* are recorded in hertz (Hz) and signal

multiplicities expressed by singlet (s), doublet (d), triplet (t), quartet (q), broad (br), multiplet (m) or doublet of doublets (dd).

Preparative RP-HPLC was carried out using phenomenex kromasil (5 µ, 100 A) reverse phase C_{18} column (250 x 21.2 mm), a flow rate of 21.20 mL min^{-1} and UV detection at 220 nm, 28% B for 20 minutes, Solvent A: 0.06% TFA in water, solvent B: 0.06% TFA in CH_3CN.

4.2 Synthesise of nanoparticle building blocks

4.2.1 *N*-(11-azido-3,6,9-trioxaundecanyl)acrylamide 11

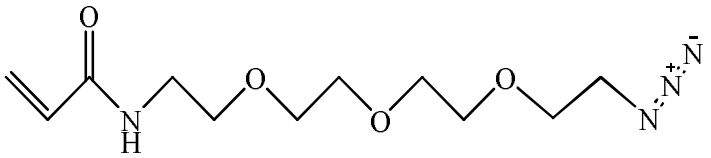

To a flame dried round bottom flask was added 11-azido-3,6,9-trioxoundecan-1-amine **14** (400 µL, 0.20 mmol) and dry DCM (5 mL). A solution of acryloyl chloride **15** (197 µL, 0.24 mmol) in dry DCM (2.5 mL) was then dropped slowly to the reaction mixture at 0 °C. After adding triethylamine (337 µL, 0.24 mmol), the yellow reaction solution was left to stir at room temperature under a nitrogen atmosphere for 4 hours. The DCM was then removed on the rotary evaporator. THF was then added and the resulting white precipitate removed by filtration. The THF was subsequently removed by rotary evaporation leaving a yellow oil which was dried *in vacuo*. The crude product was further purified by preparative HPLC yielded a yellow oil **11** (181.1 mg, 0.60 mmol, 34%). Rf = 0.05 (Hex:EtOAc = 10:90)

IR: νmax (NaCl):

3321 (m, NH), 2868 (br, aliphatic), 2103 (s, N_3), 1661 (s, C=O), 1627 (m, C=C), 1537 (s, NH), 1119 (m, C-O-C) cm^{-1}

^{1}H-NMR (δ, $CDCl_3$, 400 MHz): 6.29 (dd, *J* = 16.8/1.6 Hz, 1H, C*H*$_{trans}$=CH), 6.29 (bs, 1H, N*H*) 6.12 (dd, *J* = 16.8/10.4 Hz, 1H, C*H*=CH_2), 5.63 (dd, *J* = 10.4/1.6 Hz, 1H, C*H*$_{cis}$=CH), 3.69-3.60 (m, 12 H, C*H*$_2$-O), 3.54 (m, 2H, C*H*$_2$-NH), 3.39 (t, *J* = 5.2 Hz, 2H, C*H*$_2$-N_3)

^{13}C-NMR (δ, 100 MHz, $CDCl_3$): 165.6 (C), 131.1 (CH), 126.4 (CH), 70.8 (CH_2), 70.7 (CH_2), 70.7 (CH_2), 70.4 (CH_2), 70.2 (CH_2), 69.9 (CH_2), 50.8 (CH_2), 39.4 (CH_2).

m/*z*: 273.0926 (MH^+), calc. 273.1563

4.2.2 *N*-propargyl acrylamide 17

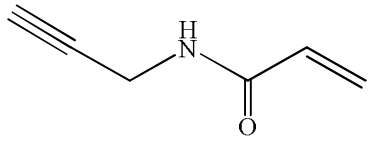

Propargylamine **18** (0.60 mL, 9.37 mmol) and *N*,*N*-diisopropylethylamine (1.95 mL, 11.24 mmol) were added to a 2 neck round bottom flask and dissolved in dry DCM (3 mL). To the mixture was then added dropwise a solution of acryloyl chloride **15** (0.910 mL, 11.20 mmol) in dry DCM (2 mL). The reaction was left to stir overnight under a nitrogen atmosphere, after which time the organic phase was removed by rotary evaporation. The crude product was subsequently dissolved in ethyl acetate and washed three times with an aqueous bicarbonate solution, two times with a brine solution and two times with distilled water. After collecting and drying the organic phase over $MgSO_4$, ethyl acetate was removed on the rotary evaporator yielding the product as a white crystalline solid **17** (367 mg, 36%). Rf = 0.7 (Hex:EtOAc = 50:50)

Melting point: 39-40°C,

IR: ν_{max} (KBr):

3293 (s, alkyne), 3234 (m, NH), 1677 (s, C=O), 1649 (s, C=C), 1545 (s, NH) cm^{-1},

^{1}H NMR (δ, 400 MHz,$CDCl_3$) : 6.32 (dd, *J* = 17.2/1.6 Hz, 1H, C*H*$_{2,trans}$=CH), 6.10 (dd, *J* = 17.2/10.4 Hz, 1H, C*H*=CH_2), 5.79 (bs, 1H, N*H*), 5.69 (dd, *J* = 10.4/1.2 Hz, 1H, C*H*$_{2,cis}$=CH), 4.14 (dd, *J* = 5.2/2.4 Hz, 1H, C*H*$_2$-NH), 2.25 (t, *J* = 2.4 Hz, 1H, C*H*-C)

^{13}C NMR (δ, 100 MHz, $CDCl_3$): 165.1 (C), 130.1 (CH), 127.3 (CH_2), 79.3 (C), 71.8 (CH), 29.3 (CH_2)

m/*z*: 110.1327 (MH^+), calc. 110.0606

4.2.3 Attempt of synthesis of *N*-(2-aminoethyl)maleimide using Mitsunobu reaction conditions.

4.2.3.1 Synthesis of *tert*-butyl 2-hydroxyethylcarbamate 24

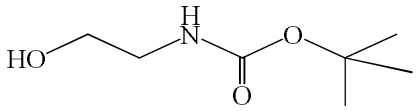

2-aminoethanol **23** (500 µL, 8.28 mmol) was added to a round bottom flask and dissolved in dry DCM (10 mL). BOC anhydride (1.64 g, 7.53 mmol) dissolved in 2 ml of DCM was added drop-wise to it. The reaction mixture was allowed to react for 3 hours. The solvent was evaporated under reduced pressure and the residue was dissolved in ethyl acetate. The organic phase was washed with citric acid (pH=4), $NaHSO_4$ and brine solutions and dried over $MgSO_4$ and filtered. The solvent was evaporated *in vacuo* and **24** was obtained as a colourless oil. (Hexane: EtOAc, 80: 20) (478.3mg, 2.3 mmol, 36%). Rf = 0.3 (Hex: EtOAc 50:50)

IR:ν_{max} (NaCl):

3360 (br, OH), 1691 (s, C=O), 1539 (s, NH),

^{1}H NMR (δ, 400 MHz, $CDCl_3$): 5.31 (br s, 1N*H*), 3.70 (t, J= 5.08 Hz, 2H), 3.30 (t, J=5.08 Hz, 2H), 1.46 (s, 9H)

^{13}C NMR (δ, 100 MHz, $CDCl_3$): 156 (C), 79.5 (C), 61.5 (CH_2), 43.1 (CH_2), 28.4 (CH_3)

m/*z*: 162.1024 (MH^+), calc. 162.1130

4.2.3.2 Attempt of synthesise of *tert*-butyl 2-(2,5-dioxo-2H-pyrrol-1(5H)-yl)ethyl carbamate 27

To a flame heated two neck round bottom flask, triphenyl phosphine (PPh_3) (515.5 mg, 1.96 mmol) and diisopropyl azodicarboxylate (DIAD) (422 µL, 2.14 mmol) were added and dissolved in tetrahydrofuran. *Tert*-butyl 2-hydroxyethylcarbamate **24** (288 mg, 1.78 mmol) was added followed by maleimide **25** (190.7 mg, 1.96 mmol). Reaction was allowed to proceed for 48 hours with continuous nitrogen supply at room temperature. THF was evaporated and the residue was triturated with diethyl ether: hexane (1:1) and the compound separated using column chromatography (hexane: ethyl acetate, 80:20). A white solid was obtained (163.2 mg), which was identified as maleimide.

Melting point: 96-98°C

IR: ν_{max} (KBr):

3051 (s, C=C), 1744 (s, C=O), 1536 (s, C=C)

^{1}H-NMR (δ, 400 MHz, $CDCl_3$): 7.95 (bs, N*H*) 6.65 (s, 2H, C=CH)

^{13}C-NMR (δ, 100 MHz, $CDCl_3$): 170.7 (C), 135.1 (CH)

m/*z*: 98.0288 (MH^+), calc. 98.0237

4.2.4.1 Synthesis of *tert*-butyl 2-(2,5-dioxo-2H-pyrrol-1(5H)-yl) ethylcarbamate 27

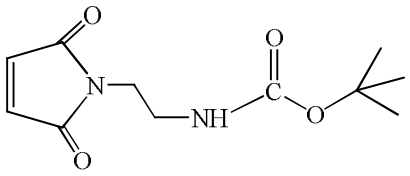

N,*N*-diisopropylethylamine (DIPEA) (1.04 mL, 6.0 mmol) and *tert*-butyl 2-aminoethylcarbamate **38** (950 µL, 6 mmol) were added in to a flame dried double neck round bottom flask and then dissolved with diethyl ether (20 mL) at 0˚C. A solution of maleic anhydride **37** (589 mg, 6 mmol) in diethyl ether was added dropwise. The reaction mixture was stirred for 6 hours while temperature reached ambient temperature. The resulting crude intermediate *N*,*N*-diisopropylethylamine salt was separated and dissolved in dichloromethane (40 mL). DIPEA (2.09 mL, 12 mmol) and TBTU (O-(1H-benzotriazole-1-yl)-*N*,*N*,*N*',*N*'-tetramethyluronium tetrafluoroborate) (1.93 g, 6 mmol) were added and stirred for another four hours. DCM was evaporated and the dark brown residue was dissolved in ethyl acetate (30 mL). The organic layer was washed with sat. $KHSO_4$, $NaHCO_3$ and brine and was evaporated after drying over $MgSO_4$. The resulted dark brown oily residue was chromatographed on silica gel (Hexane/EtOAC 1:1). A white crystalline solid **27** was obtained. (382.5 mg, 1.59 mmol, 26%). R_f =0.70 (Hex: EtOAc= 50:50)

Melting point: 110-112˚C

^{1}H NMR (δ, 400 MHz, $CDCl_3$): 6.74 (s, 2H, C=C*H*), 4.75 (bs, 1H, N*H*), 3.67 (dd, *J* = 5.44/4.36 Hz, 2H, C*H*$_2$-CH$_2$-NH), 3.35 (q, *J* =4.12 Hz, 2H, C*H*$_2$NH$_2$), 1.42 (s, 9H)

^{13}C-NMR (δ, 100 MHz, $CDCl_3$): 170.7 (C), 156.4 (C), 135.5 (CH), 79.3 (C), 46.5 (CH_2), 37.8 (CH_2), 28.0 (CH_3)

m/*z*: 241.1191 (MH^+), calc. 241.1188

4.2.4.2 Synthesis of 1-(2-aminoethyl)-1H-pyrrole-2, 5-dione 22

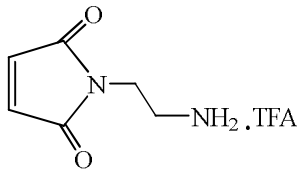

Tert-butyl 2-(2,5-dioxo-2H-pyrrol-1(5H)-yl) ethylcarbamate **27** (382.5 mg, 1.59 mmol) was dissolved in DCM (3.0 mL) and treated with trifluoroacetic acid (TFA) (9.0 mL) for 2 hours. The solution was evaporated using rotary evaporator. The residual off white solid was triturated with diethyl ether and filtered. The solid was further dried in *vacuo* to afford the title compound **22** as a TFA salt. (360.5 mg, 1.4 mmol, 89%). R_f = 0 (Hex: EtOAc = 50:50)

Melting point: 125-127°C

IR: ν_{max} (KBr):

3055 (s, C=C), 1714 (s, C=O), 1539 (s, C=C)

^{1}H-NMR (δ, 400 MHz, $CDCl_3$): 6.85 (s, 2H, C=CH), 3.78 (t, *J* = 5.16 Hz, 2H, C*H*$_2$-CH$_2$-NH), 3.19 (t, *J* =5.72 Hz, 2H, C*H*$_2$NH$_2$)

^{13}C-NMR (δ, 100 MHz, $CDCl_3$): 172.8 (C), 134.8 (CH), 38.5 (CH_2), 35.1 (CH_2)

m/*z*: 141.1614 (MH^+), calc. 141.0664

4.2.4.3 *N*-(maleimidoethyl) acrylamide 21

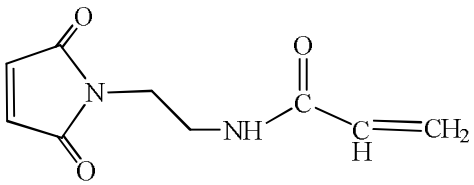

To a flame dried round bottom flask, acryloyl chloride **15** (82 µL, 1.20 mmol) and tetrahydrofuran (THF) (15 mL) were added. 1-(2-aminoethyl)-1H-pyrrole-2, 5-dione **22** (144.2 mg, 0.56 mmol) dissolved in THF was then slowly dropped in to the reaction mixture at 0 °C. After adding *N*,*N*-diisopropylethylamine (681 µL, 1.13 mmol), the yellow coloured reaction

solution was left to stir at room temperature under a nitrogen atmosphere for 10 hours. The THF was removed on the rotary evaporator and the residue was purified column chromatography giving **21** as a white solid. The resulting compound which was dried *in vacuo*. (49.6 mg, 0.25 mmol, 44%). R_f =0.07 (Hex: EtOAC= 50:50)

Melting point: 158-160°C

IR: ν_{max} (KBr):

3293 (s, NH), 3093 (s, C=C), 1702 (s, C=O), 1624 (s, C=C), 1555 (s, NH),

^{1}H NMR (δ, 400 MHz, D_2O) : 6.74 (s, C*H*=CH), 6.27 (dd, *J* = 6.56/1.36 Hz, 1H, C$H_{2,trans}$=CH), 6.10 (dd, *J* = 14.2/10.3 Hz, 1H, C*H*=CH_2), 6.0 (bs, 1H, N*H*), 5.64 (dd, *J* = 1.36/1.34 Hz, 1H, C$H_{2,cis}$=CH), 3.78 (q, *J* = 5.16 Hz, 2H, CH_2-CH_2-NH), 3.19 (m, *J* =1.6 ,2.0, 4.0) 2H, CH_2NH)

^{13}C-NMR (δ, 100 MHz, D_2O): 170.9 (C), 165.9 (C), 134.2 (CH), 130.6 (CH), 126.5 (CH_2), 39.8 (CH_2), 39.0 (CH_2)

m/*z*: 195.0925 (MH^+), calc. 195.0770

4.3 Synthesis of nanoparticles

4.3.1 Synthesis of non-functionalised nanoparticles

The surfactants, Brij 30 (1.54 g) and AOT (0.80 g) were dissolved in deoxygenated hexane (21 mL) to establish the water-in-oil microemulsion. To the mixture was then added the aqueous phase (1 mL), which consisted of the monomers acrylamide **12** (265 mg, 3.73 mmol) and and the crosslinker *N*,*N*'-methylenebisacrylamide **13** (80 mg, 0.52 mmol). The polymerisation was initiated by the addition of ammonium persulphate (APS) (15 μL, 10% w/v) and *N*,*N*,*N*',*N*'-tetramethylethylenediamine (TEMED) (7.5 μL). The reaction mixture was allowed to proceed for 2 hours while stirring under an argon atmosphere. Then the hexane was removed by rotary evaporation. An opaque, viscous residue was obtained. The particles were washed 10 times with ethanol to remove surfactants and unreacted monomers. The particles were then collected by vacuum filtration using a Millipore filtration system with a 0.02

μm anodisc filter. After drying *in vacuo*, the particles were obtained as a white powder. (278 mg, 80%). IR: ν_{max} (KBr): 1708 (s, C=O)

4.3.2 Synthesis of azide functionalized nanoparticles

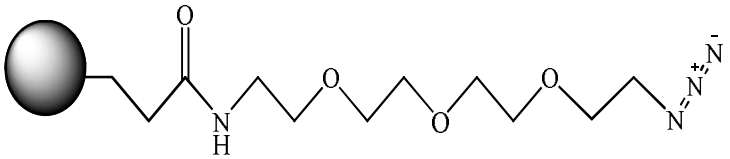

The surfactants Brij 30 (1.54 g) and AOT (0.80 g) were dissolved in deoxygenated hexane (21 mL) to establish the water-in-oil microemulsion. To the mixture was then added the aqueous phase (1 mL), which consisted of the monomers acrylamide **12** (265 mg, 3.73 mmol) and *N*-(11-azido-3,6,9-trioxaundecanyl)acrylamide **11** (13.6 mg, 0.046 mmol) and the crosslinker *N,N'*- methylene bisacrylamide **13** (80 mg, 0.52 mmol). The polymerisation was initiated by the addition of ammonium persulphate (15 μL, 10% w/v) and *N,N,N',N'*-tetramethylethylenediamine (7.5 μL). The reaction mixture was allowed to react for 2 hours while stirred under an argon atmosphere. Then the hexane was removed by rotary evaporation. An opaque, viscous residue was obtained. The particles were washed 12 times with absolute ethanol to remove surfactants and unreacted monomers. The particles were then collected by vacuum filtration using a Millipore filtration system with a 0.02 μm Anodisc filter. After drying *in vacuo* the particles were obtained as a white powder. (257 mg, 72%). IR: ν_{max} (KBr): 2110 (s, N_3), 1679 (s, C=O)

4.3.3 Synthesis of alkyne functionalized nanoparticles

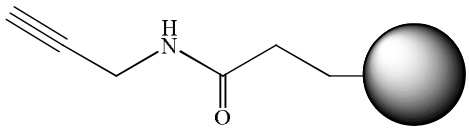

The surfactants, Brij 30 (1.54 g) and AOT (0.80 g) were dissolved in deoxygenated hexane (21 mL) to establish the water-in-oil microemulsion. To the mixture was then added the aqueous phase (1 mL), which consisted of the monomers acrylamide **12** (265 mg, 3.73 mmol) and *N*-propargyl acrylamide **17** (12 mg, 0.11 mmol) and *N,N'*-methylenebisacrylamide **13** (80 mg, 0.52 mmol). The polymerisation was initiated by the addition of ammonium persulphate (15 µL, 10% w/v) and *N,N,N',N'*-tetramethylethylenediamine (7.5 µL). The reaction mixture was allowed to react for 2 hours while stirred under an argon atmosphere. Then the hexane was removed by rotary evaporation. An opaque, viscous residue was yielded. The particles were washed 12 times with absolute ethanol to remove surfactants and unreacted monomers,. The particles were then collected by vacuum filtration using a Millipore filtration system with a 0.02 µm anodisc filter. After drying *in vacuo* the particles were obtained as a white powder. (259 mg, 73%). IR: ν_{max} (KBr): 1661 (s, C=O)

4.3.4 Synthesis of maleimide functional nanoparticles

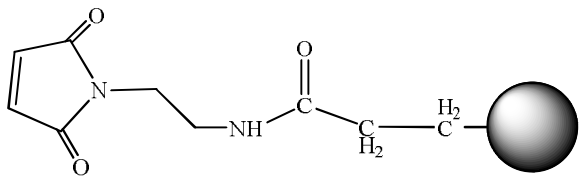

The surfactants Brij 30 (1.54 g) and AOT (0.80 g) were dissolved in deoxygenated hexane (21 mL) to establish the water-in-oil microemulsion. To the mixture was then added the aqueous phase (1 mL), which consisted of the

monomers N-(2-aminoethyl)maleimide acrylamide **21** (10 mg, 0.05 mmol), acrylamide **12** (265 mg, 3.73 mmol) and and the *N,N'*- methylenebisacrylamide **13** (80 mg, 0.52 mmol). The polymerisation was initiated by the addition of ammonium persulphate (15 μL, 10% w/v) and TEMED (*N,N,N',N'*-tetramethylethylenediamine) (7.5 μL). The reaction mixture was allowed to react for 2 hours while stirred under an argon atmosphere. Then the hexane was removed by rotary evaporation. An opaque, viscous residue was yielded. The particles were washed 12 times with absolute ethanol to remove surfactants and unreacted monomers,. The particles were then collected by vacuum filtration using a Millipore filtration system with a 0.02 μm anodisc filter. After drying *in vacuo* the particles were obtained as a white powder. (244 mg, 68%). IR: ν_{max} (KBr): 1672 (s, C=O)

4.3.6 Synthesis of alkyne functionalized nanoparticles with incorporated dextran bound TAMRA fluorophore

The surfactants Brij 30 (1.54 g) and AOT (0.80 g) were dissolved in deoxygenated hexane (21 mL) to establish the water-in-oil microemulsion. To the mixture was then added the aqueous phase (1 mL), which consisted of the monomers acrylamide **12** (265 mg, 3.73 mmol) and *N*-propargyl acrylamide **17** (12 mg, 0.11 mmol), *N,N'*-methylenebisacrylamide **13** (80 mg, 0.52 mmol), TAMRA-dextran (100 μL, 5 mg mL^{-1} solution in water) dissolved in water (800 μL) and DMSO (200 μL). The polymerisation was initiated by the addition of ammonium persulphate (15 μL, 10% w/v) and *N,N,N',N'*-tetramethylethylenediamine (7.5 μL). The reaction mixture was allowed to react for 2 hours while stirred under an argon atmosphere. Then the hexane was removed by rotary evaporation. An opaque, viscous residue was yielded. The particles were washed 12 times with absolute ethanol to remove surfactants and unreacted monomers, the particles were then collected by vacuum filtration using a Millipore filtration system with a 0.02 μm anodisc filter. After drying *in vacuo* the particles were obtained as a white powder (207 mg, 58%). IR: ν_{max} (KBr): 1706 (s, C=O)

4.4 Procedure for clicking alkyne bearing compounds to azide functionalized nanoparticles

4.4.1 Click reaction with alkyne modified TAMRA fluorophore

Alkyne modified TAMRA fluorophore (50 µL, 0.5 mg in 1 mL DMSO, 53.4 nmol) and azide functionalized nanoparticles (10 mg) were added to a vial. They were suspended in a solvent mixture of *t*-butylalcohol: water: DMSO of 45:45:10. Tetrakis(acetonitrile) copper(I) hexafluorophosphate (10 mol% with respect to alkyne modified TAMRA fluorophore , 5.34 nmol) and the Cu(I) stabilizing ligand TBTA (10 mol% with respect to alkyne modified TAMRA fluorophore, 5.34 nmol), were then added to the vial, achieved by serial dilutions in DMSO. The reaction mixture was gently stirred for 48 hours in the dark, after which time the particles were washed with DMF (15 times, 1.5 mL) and EtOH (15 times, 1.5 mL) by centrifugation. The pinkish particles were subsequently dried *in vacuo* (8 mg). The negative control reaction was identical to above, except unmodified poly(acrylamide) nanoparticles were used.

4.4.2 Click reaction with Z-Gly-Gly-Leu-ACA-Lys(pentynamide)-NH_2

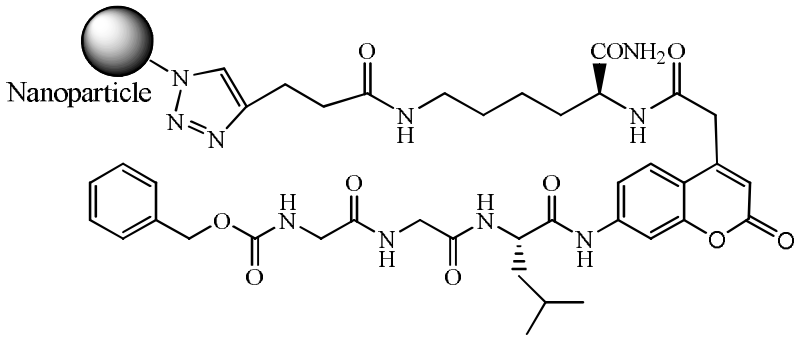

Z-Gly-Gly-Leu-ACA-Lys(pentynamide)-NH_2 (1.5 mg, 1.90 µmol) and azide functionalized nanoparticles (17 mg) were added to a vial and were suspended in a solvent mixture of water:*t*-butylalcohol:DMSO of 45:45:10. Tetrakis(acetonitrile) copper(I) hexafluorophosphate (10 mol% with respect to alkyne modified fluorophore, 190 nmol) and TBTA (10 mol% with respect to alkyne modified fluorophore, 190 nmol), were then added to the vial, achieved by serial dilutions in DMSO. The suspension was gently stirred for 48 hours in

the dark, after which time the particles were washed with DMF (15 times, 1.5 mL) and EtOH (15 times, 1.5 mL) by centrifugation. After drying *in vacuo*, the particles were obtained as a white powder (18 mg). The negative control reaction was identical to above, except unmodified poly(acrylamide) nanoparticles were used.

4.5 Procedure for clicking azide bearing compounds to alkyne functionalized nanoparticles

4.5.1 Click reaction with 2-azido-acetyl-lysin(5-carboxyfluoresceinyl)-amide

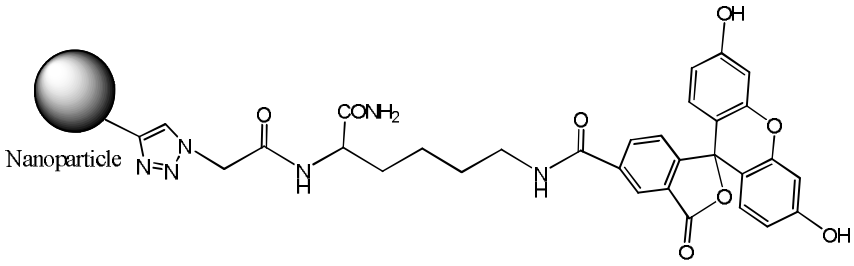

Alkyne functionalized nanoparticles (20 mg) and 2-azido-acetyl-lysin(5-carboxyfluoresceinyl)-amide (2.5 mg, 4.25 μmol) were added to a vial and were subsequently suspended in a solvent mixture of water:*t*-butylalcohol:DMSO of 70:20:10. To the vial was then added (acetonitrile)copper(I) hexafluorophosphate (7 mol% with respect to azido functionalized fluorophore, 295 nmol) and TBTA (7 mol% with respect to azido functionalized fluorophore, 295 nmol), achieved by serial dilutions in DMSO. The reaction mixture was gently stirred for 48 hours in the dark, after which time the particles were washed with DMF (15 times, 1.5 mL) and EtOH (15 times, 1.5 mL) by centrifugation. After drying *in vacuo*, the particles were obtained as a white powder (19 mg). The negative control reaction was identical to above, except unmodified poly(acrylamide) nanoparticles were used.

4.6 Thiol-maleimide click reaction for clicking thiol modified fluorophore to maleimide functionalized nanoparticles

Maleimide functional nanoparticles (20 mg) were added to the round bottom flask and dissolved in DMF (5 mL). Triethylamine (1 μL, 7.2 μmol) and cysteine modified carboxyfluorescein **46** (6.7 mg, 0.01 mmol) were added and allowed to react for 24 hours while stirring. After which time, the particles were washed with DMF (18 times, 2.5 mL) by centrifugation. After drying *in vacuo*, the particles were obtained as a white powder (19mg). The negative control reaction was identical to above, except unmodified poly(acrylamide) nanoparticles were used.

4.8 Calculations

4.8.1 Calculation of remaining maleimide functional groups in nanoparticles

Known concentrations of cysteine modified carboxyfluorescein solution series were preapared and their maximum fluorescence units were measured (table 2.3.2).

Table 4.1: Fluorescence Vs known concentrations of cysteine modified carboxyfluorescein.

Concentration ($1x10^{-3}$ mg/mL)	Concentration (nmol/mL)	Maximum fluorescence unit (a.u)
1.25	2.6	76.43
1.00	2.0	65.76
0.50	1.0	43.10
0.25	0.5	14.74
0.16	0.3	08.40

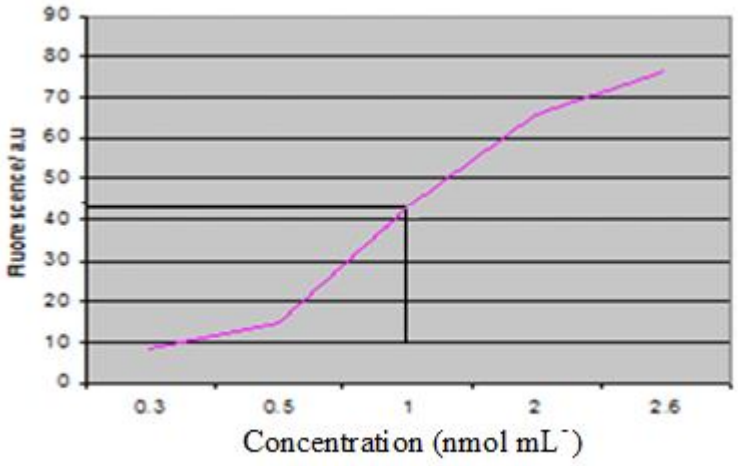

Figure 4.1: Fluorescence vs. known concentration of cysteine modified carboxyfluorescein.

Maximum observed fluorescence units for the prepared 1 mg ml^{-1} nanoparticle solution = 43.23 a.u

According to the plot, concentration of the cysteine modified carboxyfluorescein of the nanoparticle solution = 1.02 nmol mL^{-1}

Therefore available maleimide functional moles in 1 mg/mL

of nanoparticle Solution = 1.02 nmol

4.8.2 Availability of maleimide functional groups

Amount of maleimide monomer used for the polymerisation= 10 mg

Molecular weight of the maleimide monomer = 194. 18 g/mol

Number of moles used for the polymerisation = 10 x 10^{-3} g/ 194.18 g/mol

= 5.15 X 10^{-5} mol

Yield of the nanoparticles = 244 mg

Yield % of the nanoparticles = 68%

Therefore, the number of maleimide moles included in the nanoparticles

= 5.15 X 10^{-5} X 68 % mol

= 3.5 X 10^{-5} mol

Number of maleimide monomer moles in 1 mg of nanoparticles

$= 3.5 \text{ X } 10^{-5} \text{ mol} / 244$

$= 140 \text{ nmol}$

The percentage of the available nanoparticles $= (1.02/ 140) \text{ x } 100 \%$

$= 0.7 \%$

So the polymerised percentage of maleimide functional groups

$= 100\% - 0.7 \% = 99.3 \%$

References

1. Riley, T., Heald, C. R., Stolnik, S., Garnett, M. C., Illum, L., Davis, S. S., King, S. M., Heenan, R. K., Purkiss, S. C., Barlow, R. J., Gellert, P. R., Washington, C., (2003) Core-shell structure of PLA-PEG nanoparticles used for drug delivery. *Langmuir 19*, 8428-8435.
2. Lee, S., Park, K., Kim, K., Choi, K., Kwon, I. C., (2008) Activatable imaging probes with amplified fluorescent signals. *Chem. Commun.* 36, 4250-4260.
3. Borisov, S. M., Klimant, I., (2008) Optical nanosensors - Smart tools in bioanalytics. *Analyst* 133, 1302-1307.
4. Aylott, J. W., (2003) Optical nanosensors - an enabling technology for intracellular measurements. *Analyst* 128, 309-312.
5. Clark, H. A., Barker, S. L. R., Brasuel, M., Miller, M. T., Monson, E., Parus, S., Shi, Z. Y., Song, A., Thorsrud, B., Kopelman, R., Ade, A., Meixner, W., Athey, B., Hoyer, M., Hill, D., Lightle, R., Philbert, M. (1998) Subcellular optochemical nanobiosensors: probes encapsulated by biologically localised embedding (PEBBLEs). *Sensors and Actuators* 51, 12-16.
6. Cao, Y. F., Koo, Y. E. L., Kopelman, R., (2004) Poly(decyl methacrylate)-based fluorescent PEBBLE swarm nanosensors for measuring dissolved oxygen in biosamples. *Analyst* 129, 745-750.
7. Sumner, J. P., Aylott, J. W., Monson, E., Kopelman, R., A (2002) fluorescent PEBBLE nanosensor for intracellular free zinc. *Analyst* 127, 11-16.
8. Uhlmann, D. R., Teowee, G., (1998) Sol-gel science and technology: Current state and future prospects. *J Sol-Gel Sci Technol.* 13, 153-162.
9. Xu, H., Aylott, J. W., Kopelman, R., (2002) Fluorescent nano-PEBBLE sensors designed for intracellular glucose imaging. *Analyst* 127, 1471-1477.
10. McNamara, K. P., Rosenzweig, Z., (1998) Dye-encapsulating liposomes as fluorescence-based oxygen nanosensors. *Anal. Chem.*70, 4853-4859.

11. Ji, J., Rosenzweig, N., Griffin, C., Rosenzweig, Z., (2000) Synthesis and application of submicrometer fluorescence sensing particles for lysosomal pH measurements in murine macrophages. *Anal. Chem.*72, 3497-3503.
12. Allard, E., Larpent, C., (2008) Core-shell type dually fluorescent polymer nanoparticles for ratiometric pH-sensing. *J polym. Sci.* 46, 6206-6213.
13. Coupland, P. G., Fisher, K. A., Jones, D. R. E., Aylott, J. W., (2008) Internalisation of polymeric nanosensors in mesenchymal stem cells: Analysis by flow cytometry and confocal microscopy. *J. Control. Release* 130, 115-120.
14. Green, K., Brand, M. D., Murphy, M. P., (2004) Prevention of mitochondrial oxidative damage as a therapeutic strategy in diabetes. *Diabetes* 53, 110-112.
15. Jung, S. K., Kauri, L. M., Qian, W. J., Kennedy, R. T., (2000) Correlated oscillations in glucose consumption, oxygen consumption, and intracellular free Ca2+ in single islets of Langerhans. *J. Biol. Chem.* 275, 6642-6650.
16. Webster, A., Coupland, P., Houghton, F. D., Leese, H. J., Aylott, J. W., (2007) The delivery of PEBBLE nanosensors to measure the intracellular environment. *Biochem. Soc. Trans* 35, 538-543.
17. Klein, T. M., Wolf, E. D., Wu, R., Sanford, J. C., (1987) High-velocity microprojectiles for delivering nucleic-acids into living cells. *Nature* 32, 770-73.
18. Stewart, K. M., Horton, K. L., Kelley, S. O., (2008) Cell-penetrating peptides as delivery vehicles for biology and medicine. *Org. Biomol. Chem.* 6, 2242-2255.
19. Frankel, A. D., Pabo, C. O., (1988) Cellular uptake of the tat protein from human immunodeficiency virus. *Cell* 55, 1189-1193.
20. Kerkis, A., Hayashi, M. A. F., Yamane, T., Kerkis, I., (2006) Properties of cell penetrating peptides (CPPs*). IUBMB Life* 58, 7-13.
21. Zhao, M., Kircher, M. F., Josephson, L., Weissleder, R., (2002) Differential conjugation of tat peptide to superparamagnetic

nanoparticles and its effect on cellular uptake. *Bioconjugate Chem.* 13, 840.

22. Kersemans, V., Kersemans, K., Cornelissen, B., (2008) Cell penetrating peptides for in vivo molecular imaging applications. *Curr. Pharm. Des.* 14, 2415-2427.
23. Schwarze, S. R., Ho, A., Vocero-Akbani, A., Dowdy, S. F., (1999) In vivo protein transduction: Delivery of a biologically active protein into the mouse. *Science* 285, 1569-1572.
24. Leong, Y. S., Candau, F., (1982) Inverse micro-emulsion polymerization. *J Phys. Chem.* 86, 2269-2271.
25. Zhang, Q. Y., Bao, X. J., Lin, M., Hourston, D. J., (2006) Preparation of nanometer-sized poly(methacrylic acid) particles in water-in-oil microemulsions. *J. Appl. Polym. Sci* 100, 2497-2503.
26. Hao, J. C., (2001) Microemulsion polymerization of acrylamide and styrene: Effect of the structures of reaction media. *J. Polym Sci* 39, 3320-3334.
27. Juranicova, V., Kawamoto, S., Fujimoto, K., Kawaguchi, H., Barton, J., (1998) Inverse microemulsion polymerization of acrylamide in the presence of N,N-dimethylacrylamide. *Angew. Chem., Int. Ed* 258, 27-31.
28. Arriagada, F. J., Osseo-Asare, K., (1999) Synthesis of nanosize silica in a nonionic water-in-oil microemulsion: Effects of the water/surfactant molar ratio and ammonia concentration. *J. Colloid Interface Sci.* 211, 210-220.
29. Goyal, P. S., Aswal, V. K., (2001) Micellar structure and inter-micelle interactions in micellar solutions: Results of small angle neutron scattering studies. *Curr. Sci.* 80, 972-979.
30. Moulik, S. P., (1996) Micelles: Self-organized surfactant assemblies. *Curr. Sci.* 71, 368-376.
31. Yildiz, G., Catalgil-Giz, H., Kadirgan, F., (2000) Electrochemically prepared acrylamide/N,N'-methylene bisacrylamide gels. *J Appl. Electrochemistry* 30, 71-75.

32. Zhang, X., Liu, W. H., Chen, Y. M., Gong, A. J., Chen, C. F., Xi, F., (1999) Self-condensing vinyl polymerization of acrylamide. *Polym. Bull.* 43, 29-34.

33. Gelfi, C., Righetti, P. G., (1981) Polymerization kinetics of polyacrylamide gels .1. Effect of different cross-linkers. *Electrophoresis* 213-219.

34. Hepworth, S. J., Leach, M. O., Doran, S. J., (1999) Dynamics of polymerization in polyacrylamide gel (PAG) dosimeters: (II) modelling oxygen diffusion. *Phys. Med. Biol.* 44, 1875-1884.

35. Turk, B., (2006) Targeting proteases: successes, failures and future prospects. *Nat. Rev.* 5, 785-799.

36. Fujinaga, M., Cherney, M. M., Oyama, H., Oda, K., James, M. N. G., (2004) the molecular structure and catalytic mechanism of a novel carboxyl peptidase from Scytalidium lignicolum. *Proc. Natl. Acad. Sci. U.S.A.* 101, 3364-3369.

37. Croney, J. C., Jameson, D. M., Learmonth, R. P., (2001) Fluorescence spectroscopy in biochemistry: teaching basic principles with visual demonstrations. *Biochem. Mol. Biol. Ed* 29, 60-65.

38. Royer, C. A., (1995) Approaches to teaching fluorescence spectroscopy. *Biophys. J.* 68, 1191-1195.

39. Baruch, A., Jeffery, D. A., Bogyo, M., (2004) Enzyme activity - it's all about image. *Trends Cell Biol.* 14, 29-35.

40. Sheehan, J. C., Hess, G. P., (1955) A new method of forming peptide bonds. *J. Am. Chem. Soc.* 77, 1067-1068.

41. Mantovani, G., Lecolley, F., Tao, L., Haddleton, D. M., Clerx, J., Cornelissen, J., Velonia, K., (2005) Design and synthesis of N-maleimido-functionalized hydrophilic polymers via copper-mediated living radical polymerization: A suitable alternative to PEGylation chemistry. *J. Am. Chem. Soc.* 127, 2966-2973.

42. Evans, R. A., (2007) The rise of azide-alkyne 1,3-dipolar 'click' cycloaddition and its application to polymer science and surface modification. *Aust. J. Chem*, 60, 384-395.

43. Geng, J., Lindqvist, J., Mantovani, G., Haddleton, D. M., (2008) Simultaneous copper(I)-catalyzed azide-alkyne cycloaddition (CuAAC)

and living radical polymerization. *Angew. Chem., Int. Ed* 47, 4180-4183.

44. Rostovtsev, V. V., Green, L. G., Fokin, V. V., Sharpless, K. B., (2002) A stepwise Huisgen cycloaddition process: Copper(I)-catalyzed regioselective "ligation" of azides and terminal alkynes. *Angew. Chem., Int. Ed.* 41, 2596

45. Himo, F., Lovell, T., Hilgraf, R., Rostovtsev, V. V., Noodleman, L., Sharpless, K. B., Fokin, V. V., (2005) Copper(I)-catalyzed synthesis of azoles. DFT study predicts unprecedented reactivity and intermediates. *J. Am. Chem. Soc.* 127, 210-216.

46. Coupland, P. G., Fisher, K. A., Jones, D. R. E., Aylott, J. W., (2008) Internalisation of polymeric nanosensors in mesenchymal stem cells: Analysis by flow cytometry and confocal microscopy. *J. Control. Release* 130, 115-120.

47. Kolb, H. C., Finn, M. G., Sharpless, K. B., (2001) Click chemistry: Diverse chemical function from a few good reactions. *Angew. Chem., Int. Ed.* 40, 2004.

48. Pounder, R. J., Stanford, M. J., Brooks, P., Richards, S. P., Dove, A. P., (2008) Metal free thiol-maleimide 'Click' reaction as a mild functionalisation strategy for degradable polymers. *Chem. Commun.* 41 5158-5160.

49. Dondoni, A., (2008) Emergence of Thiol-Ene Coupling as a Click Process for Materials and Bioorganic Chemistry. *Angew. Chem., Int. Ed.* 47, 8995-8997.

50. Zhang, J., Yu, J., Guo, Z. X., (2006) Modification of nano-alumina surface by Michael addition reaction. *Chi. Chem.l Lett.* 17, 251-252.

51. Roberts, M. J., Bentley, M. D., Harris, J. M., (2002) Chemistry for peptide and protein PEGylation. *Adv Drug Deliv Rev* 54, 459-476.

52. Tornoe, C. W., Christensen, C., Meldal, M., (2002) Peptidotriazoles on solid phase: [1,2,3]-triazoles by regiospecific copper(I)-catalyzed 1,3-dipolar cycloadditions of terminal alkynes to azides. *J. Org. Chem.* 67, 3057-3064.

53. Valverde, I. E., Delmas, A. F., Aucagne, V., (2009) Robust semi-orthogonal alkyne protecting groups for multiple successive azide/alkyne cycloadditions. *Tetrahedron* 65, 7597-7602.

54. Naoi, M., Maruyama, W., Yi, H., Akao, Y., Yamaoka, Y., Shamoto-Nagai, M., (2007) Neuroprotection by propargylamines in Parkinson's disease: intracellular mechanism underlying the anti-apoptotic function and search for clinical markers. *J Neural Transm.* 121-131.

55. Ghosh, S. S., Kao, P. M., McCue, A. W., Chappelle, H. L., (1990) Use of Maleimide-Thiol Coupling Chemistry for Efficient Syntheses of Oligonucleotide-Enzyme Conjugate Hybridization Probes. *Bioconj. Chem.* 1, 71-76.

56. Le Sann, C., (2006) Maleimide spacers as versatile linkers in the synthesis of bioconjugates of anthracyclines. *Nat. Prod. Rep.*23, 357-367.

57. King, H. D., Dubowchik, G. M., Walker, M. A., (2002) Facile synthesis of maleimide bifunctional linkers. *Tetra. Lett.* 43, 1987-1990.

58. Kotha, S., Meshram, M., Tiwari, A., (2009) Advanced approach to polycyclics by a synergistic combination of enyne metathesis and Diels-Alder reaction. *Chem. Soc. Rev.*38, 2065-2092.

59. Elson, K. E., Jenkins, I. D., Loughlin, W. A., (2003) The Hendrickson reagent and the Mitsunobu reaction: a mechanistic study. *Org. Biomol. Chem.* 1, 2958-2965.

60. Golantsov, N. E., Karchava, A. V., Yurovskaya, M. A., (2008) The Mitsunobu reaction in the chemistry of nitrogen-containing heterocyclic compounds. *Chem. Heterocycl.* 44, 263-294.

61. Hughes, D. L., Reamer, R. A., Bergan, J. J., Grabowski, E. J. J., (1988) A mechanistic study of the mitsunobu esterification reaction. *J. Am. Chem. Soc.* 110, 6487-6491.

62. Saylik, D., Horvath, M. J., Elmes, P. S., Jackson, W. R., Lovel, C. G., Moody, K., (1999) Preparation of isocyanates from primary amines and carbon dioxide using Mitsunobu chemistry. *J. Org. Chem.* 64, 3940-3946.

63. Agami, C., Couty, F., (2002) The reactivity of the N-Boc protecting group: an underrated feature. *Tetrahedron* 58, 2701-2724.

64. Han, G., Tamaki, M., Hruby, V., (2001) Fast, efficient and selective deprotection of the tert-butoxycarbonyl (Boc) group using HCl/dioxane (4 M). *J. Peptide Res* 58, 338-341.

65. Kane, B. E., Grant, M. K. O., (2008) El-Fakahany, E. E., Ferguson, D. M., Synthesis and evaluation of xanomeline analogs - Probing the wash-resistant phenomenon at the M-1 muscarinic acetylcholine receptor. *Bioorg. Med. Chem.* 16, 1376-1392.

66. Thaqi, A., McCluskey, A., Scott, J. L., (2008) A mild Boc deprotection and the importance of a free carboxylate. *Tetra. Lett.*49, 6962-6964.

67. Farha, O. K., Julius, R. L., Hawthorne, M. F., (2006) Synthesis of a homotrifunctional conjugation reagent based on maleimide chemistry. *Tetra. Lett.*47, 2619-2622.

68. Van der Veken, P., Dirksen, E. H. C., Ruijter, E., Elgersma, R. C., Heck, A. J. R., Rijkers, D. T. S., Slijper, M., Liskamp, R. M. J., (2005) Development of a novel chemical probe for the selective enrichment of phosphorylated serine- and threonine-containing peptides. *CheBbioChem* 6, 2271-2280.

69. Marder, O., Albericio, F., (2003) Industrial application of coupling reagents in peptides. *Chimica Oggi-Chemistry Today* 21, 35-40.

70. Kakuchi, T., Kusuno, A., Shibata, M., Nakato, T., (1999) Synthesis and radical polymerization of end-methacrylated poly(succinimide) leading to poly(aspartic acid) hydrogel. *Macromol. Rapid Commun.* 20, 410-414.

71. Morphy, J. R., Rankovic, Z., York, M., (2002) One-pot Hofmann elimination-transesterification/amidation reactions on REM resin using perfluorous solvents. *Tetra. Lett.*43, 6413-6415.

72. Alhambra, C., Castro, J., Chiara, J. L., Fernandez, E., Fernandez-Mayoralas, A., Fiandor, J. M., Garcia-Ochoa, S., Martin-Ortega, M. D., (2001) An improved two-resin method for the cleavage of tertiary amines from REM resin. *Tetra. Lett.*42, 6675-6678.

73. Lou, F. W., Xu, J. M., Liu, B. K., Wu, Q., Pan, Q., Lin, X. F., (2007) Highly selective anti-Markovnikov addition of thiols to vinyl ethers under solvent- and catalyst-free conditions. *Tetra. Lett.*48, (8815-8818.